*J. Fluid Mech.* (1967), *vol.* 30, *part* 4, *pp.* 741–773
*Printed in Great Britain*



# The structure of turbulent boundary layers

By S. J. KLINE, W. C. REYNOLDS, F. A. SCHRAUB† AND P. W. RUNSTADLER‡
Department of Mechanical Engineering, Stanford University

(Received 21 February 1967 and in revised form 26 July 1967)

Extensive visual and quantitative studies of turbulent boundary layers are described. Visual studies reveal the presence of surprisingly well-organized spatially and temporally dependent motions within the so-called 'laminar sublayer'. These motions lead to the formation of low-speed streaks in the region very near the wall. The streaks interact with the outer portions of the flow through a process of gradual 'lift-up', then sudden oscillation, bursting, and ejection. It is felt that these processes play a dominant role in the production of new turbulence and the transport of turbulence within the boundary layer on smooth walls.

Quantitative data are presented providing an association of the observed structure features with the accepted 'regions' of the boundary layer in non-dimensional co-ordinates; these data include zero, negative and positive pressure gradients on smooth walls. Instantaneous spanwise velocity profiles for the inner layers are given, and dimensionless correlations for mean streak-spacing and break-up frequency are presented.

Tentative mechanisms for formation and break-up of the low-speed streaks are proposed, and other evidence regarding the implications and importance of the streak structure in turbulent boundary layers is reviewed.

## 1. Introduction

The structure of any turbulent flow reflects the local balance of production, transport, and dissipation of turbulent kinetic energy. In turbulent boundary layers production plays a primary role, and hence it is important that the mechanisms of production be well understood. Since production is concentrated in the regions very near the wall, knowledge of the turbulence structure in this region is of special importance. This region is usually rather thin, and even partially complete quantitative information has been difficult to obtain by conventional techniques. In this paper we report the results of an extended study of the structure of turbulent boundary layers, with particular emphasis on the wall regions. The study is unique to the extent that the novel techniques employed afforded the opportunity to obtain combined visual and quantitative information on the motions within the boundary layer including the layers closest to the wall.

The importance of the region near the wall is clearly evidenced by the distribution of the turbulent energy production rate per unit volume across the boundary

† Now at General Electric Co., San Jose, California.
‡ Now at the Thayer School of Engineering, Dartmouth College.

layer. Figure 1*a* shows Klebanoff's (1954) production measurements and the associated regions of the boundary layer. Note that a sharp peak of production occurs just outside of the so-called 'laminar sublayer', in the 'buffer layer', that is, between the sublayer and the logarithmic portion of the velocity profile. The cumulative turbulence energy production, integrated outward from the wall,

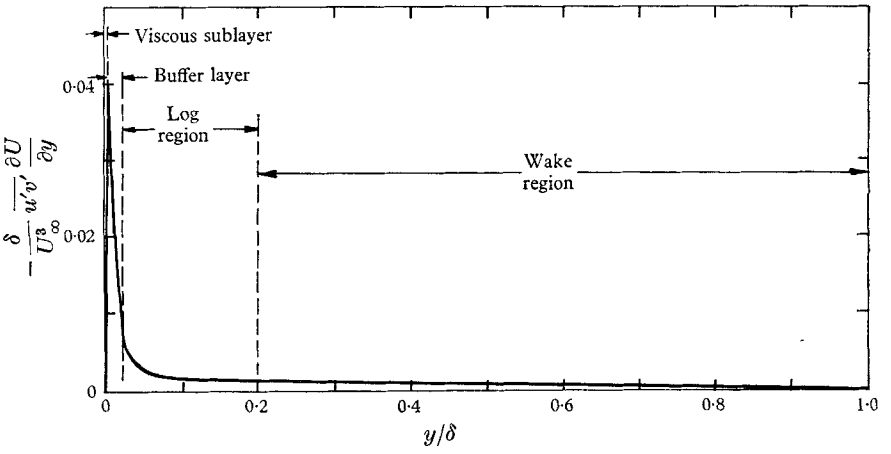


FIGURE 1*a*. Normalized turbulence energy production rate per unit volume in a typical boundary layer (Klebanoff 1954).

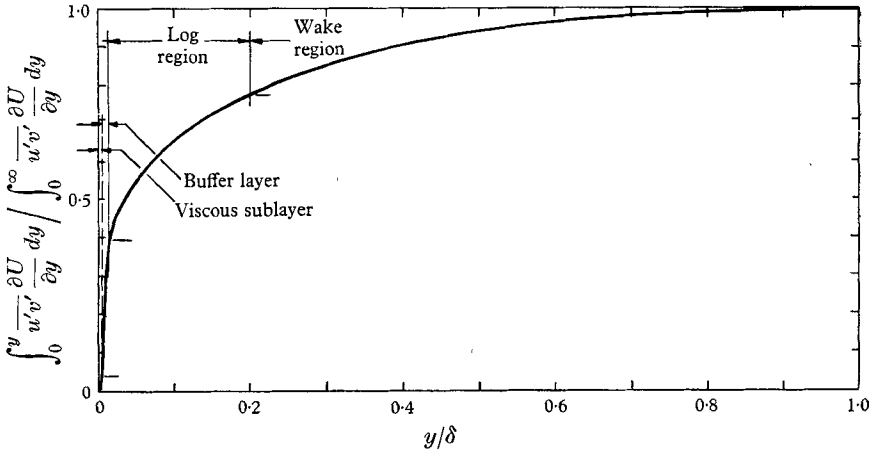


FIGURE 1*b*. Cumulative turbulence energy production rate in a typical turbulent boundary layer (Klebanoff 1954).

is shown in figure 1*b*. Note that roughly half of the total production occurs within the regions very close to the wall, and that the outer 80 % or so of the boundary layer, the wake, contributes only about 20 % to the total production. These observations are in qualitative accord with Laufer's (1954) measurements in pipe flow, and they support the contention that the thin wall region plays a very dominant role in determining the structure of the entire boundary layer.

The volumetric rate of turbulent energy production $\mathscr{P}$ also provides an important link between the volumetric rate of energy dissipation by the mean

velocity field, $\mathscr{D}$, the scalar kinematic eddy-viscosity, $\epsilon$, and the (kinematic) molecular viscosity, $\nu$,

$$\epsilon/\nu = \mathscr{P}/\mathscr{D}.$$

This is a local identity (Kline 1965*a*). Knowledge of $\epsilon$ allows calculation of the mean field from the equations of motion, and $\mathscr{D}$ is expressible in terms of the mean field. Hence, given $\mathscr{P}$ locally the mean field can be determined. This also suggests a strong focus on the production mechanisms in turbulent boundary layers.

The combined visual and quantitative techniques employed reveal a number of significant features of turbulent boundary layers; two of these particularly deserve early mention. First, the 'laminar sublayer' is not two-dimensional and steady, as simple models have sometimes assumed; rather it contains three-dimensional unsteady motions and these motions remain a large fraction of the local mean velocity right down to the wall. While the motions in this region are indeed dominated by viscosity, 'eddy' motions are present throughout the entire wall region. Secondly, it appears that a primary mechanism for production of turbulent kinetic energy in the inner region of the boundary layer is the rather violent ejection of low-speed fluid from the regions very near the wall. These 'bursts' are highly suggestive of an instability mechanism, and also appear to play a key role in transporting turbulent kinetic energy to the outer (wake) regions of the boundary layer. A positive pressure gradient tends to make the bursting more violent and more frequent; on the other hand, negative pressure gradients reduce the rate of bursting. In a sufficiently accelerated flow, the bursting ceases entirely, and the boundary layer 'relaminarizes'.

While these studies do provide new understanding of the processes occurring within a turbulent boundary layer, they also serve to re-emphasize the very complex nature of such flows, the naïveté of oversimplified flow models, and the need for additional data on actual flow models of turbulence production for various types of flows.

## 2. Experimental methods

The experiments were performed in two open-surface recirculating water channels, shown schematically in figure 2. In an early series of experiments a false floor in the larger channel was used as a flat plate. Subsequently a false sidewall in the narrower channel was used for studies in a variety of accelerating and decelerating flows.† Water speeds of the order of 0·2–0·7 ft./sec were employed; these provided quite thick boundary layers over much of the 18 ft. length of the active surfaces. The velocity data reported herein were all obtained in the narrower channel, which utilized a curved opposing wall to control the imposed pressure distribution. Water depths of the order of 10 in. were used, with the maximum channel flow width being of the order of 12 in. The channels were constructed of lucite to facilitate visualization, and care was taken to eliminate problems of vibration, unsteadiness, and temperature variation. Artificial tripping was provided upstream of the test section.

† The earlier work is described in more detail by Runstadler *et al.* (1963); the later work is reported in detail by Schraub & Kline (1965*a*). These reports will henceforth be denoted as I and II, respectively.

Mean velocity measurements were obtained using a precision constant temperature linearized hot-wire anemometer especially designed for used in low-speed water flows.† Platinum wires of 0·0008 in. diameter and approximately $\frac{1}{8}$ in. long welded to platinum leads formed the sensing element. These were

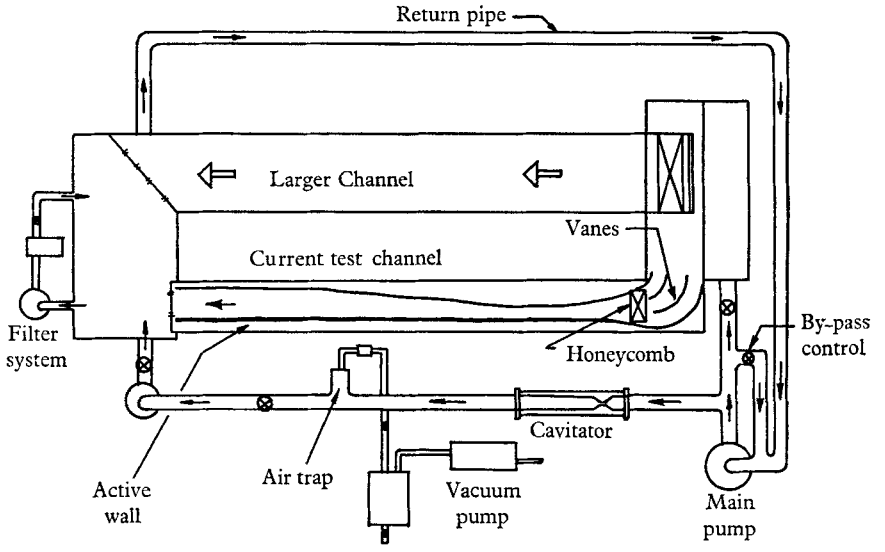


FIGURE 2. Flow system.

operated at low overheats (30 °F) in de-aerated water. The platinum–platinum system avoids stray galvanic currents; the low water conductivity reduces stray conduction; and the de-aeration and low overheat prevent air bubble formation on the wires. Because of the low overheat, low-noise high-gain amplifiers were used in the control system, and an accurate analogue linearizer was developed. At the low speeds involved the energetic fluctuation frequencies are in the range 5–100 c/s, which made conventional r.m.s. averaging equipment difficult to use. Hence the linearized signal output was integrated for 30 sec using a precision analogue integrator, and this integrated voltage was used to determine the mean velocity. Calibration velocities were determined by measuring the shedding frequency of Kármán vortices behind thin circular rods placed in a uniform flow, and using established relationships between this frequency, the flow velocity, and the fluid properties. This technique was checked by measuring the time required for dye markers to travel down several feet of the channel. As a check on the anemometer, the velocity profile in a laminar flat-plate boundary layer was measured, and its comparison with the Blasius solution for a comparable displacement thickness is shown in figure 3*a*. On the basis of this check, drift tests, and other analysis, we estimate that the uncertainty in a single mean-velocity measurement is less than 2 % for the data reported herein (20 : 1 odds).

Initial visualization experiments (I) utilized dye injection through thin slots

† See Sabin (1965), Uzkan & Reynolds (1967). This device underwent several stages of improvement and refinement; most of the data reported here were taken with the unit as modified by Uzkan.

in the wall. These studies were instrumental in revealing the essential features of the flow structure very near the wall. Subsequently visualization using tiny hydrogen bubbles was adopted since this method provides both qualitative and

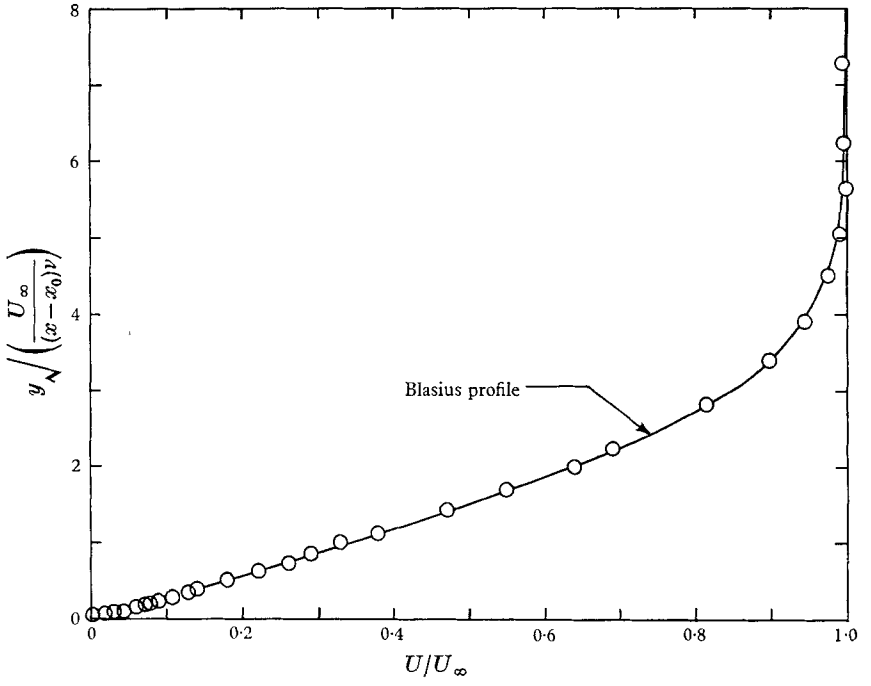


FIGURE 3*a*. Test of the hot wire in a laminar flow. ○, hot-wire data; $x_0$, effective origin found by fit.

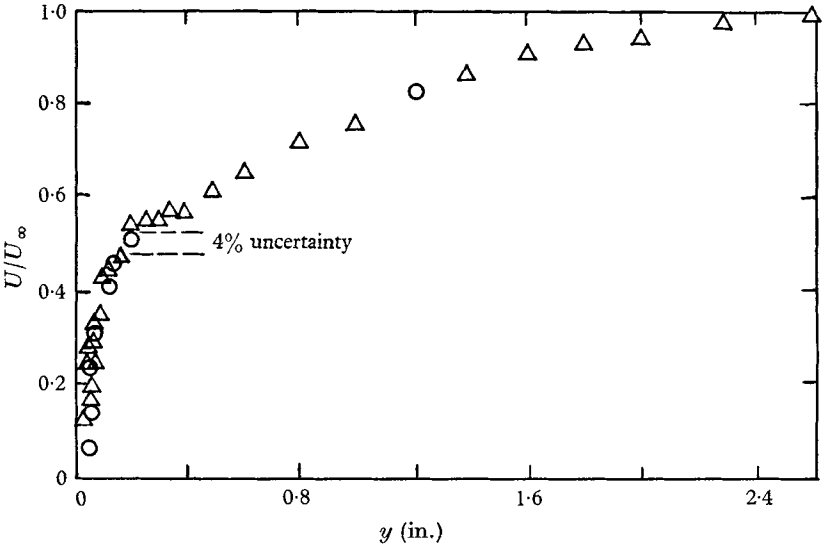


FIGURE 3*b*. Comparison of mean velocity data from hot-wire and bubble techniques. Station 10, $dP/dx \gg 0$. △, hot wire; ○, hydrogen bubble.

quantitative information. In this technique,† a single platinum wire about 6 in. long and 0·001 in. in diameter is used as an electrode to generate small ($\approx 0{\cdot}0005$ in. diameter) hydrogen bubbles. By pulsing the voltage applied to the wire, time-lines can be generated, and, by insulating spanwise portions of the wire, streaks are formed. These combined-time-streak markers can be seen in figure 10, plates 1 to 4; in each figure the wire is at the top of the picture, the flow is from the top, and the view is towards the wall.

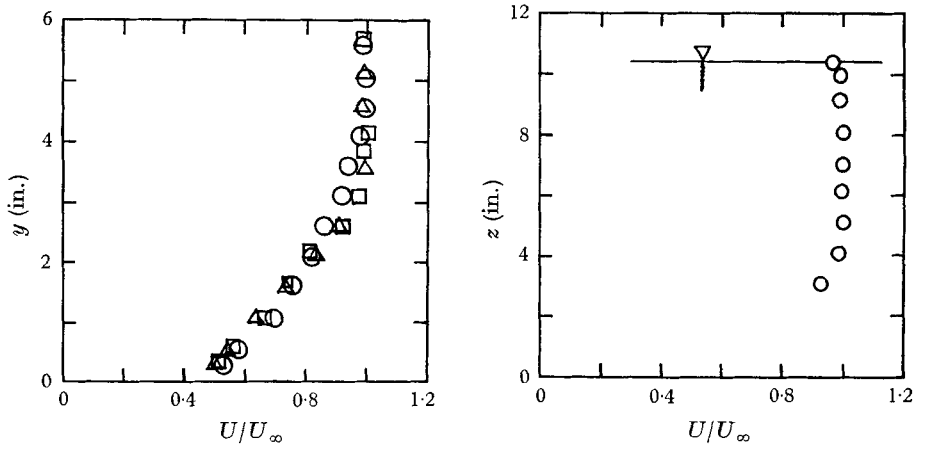


FIGURE 4. Representative checks on the two-dimensionality of the flow. Station 12, $dP/dx \gg 0$ (worst case), $y = 4{\cdot}50$ in. ○, $z = 10$ in.; △, $z = 7{\cdot}7$ in.; □, $z = 5{\cdot}5$ in.

These markers not only allow a large portion of the flow to be visualized, but can also be used to determine the instantaneous velocity distribution along the wire. A comprehensive treatment of the uncertainty in these measurements is given by Schraub *et al.* (1965*b*). For the present measurements, the estimated uncertainty in a single realization of the streamwise velocity is of the order of 2–4 % (20 : 1 odds); the highest value occurs in the region very near the wall. A comparison of the mean velocity (spanwise average) obtained using the bubble methods with the velocity (time average) measured with the hot wire is shown in figure 3*b*. These data correspond to a severe adverse pressure gradient, where the fluctuations are large, and hence the inaccuracies are greatest. The excellent agreement of these two independent techniques provides considerable basis for confidence in the instantaneous velocity measurements as deduced from motion pictures of the time-streak markers.

The two-dimensionality of the flow in the test region was checked by appropriate velocity surveys. Typical results for a strong adverse pressure gradient, the worst case, are shown in figure 4. Here $y$ is the distance normal to the wall, and $z$ is the spanwise direction. These surveys indicate that in the worst case the floor boundary layer extends upward only to about $z = 4{\cdot}5$ in. and hence the flow in

† See Schraub *et al.* (1965*b*), for a detailed description of the measurement of velocity by hydrogen bubble generation technique, and the film by Kline (1964) for a basic treatment of flow visualization with illustrations using the hydrogen bubble methods.

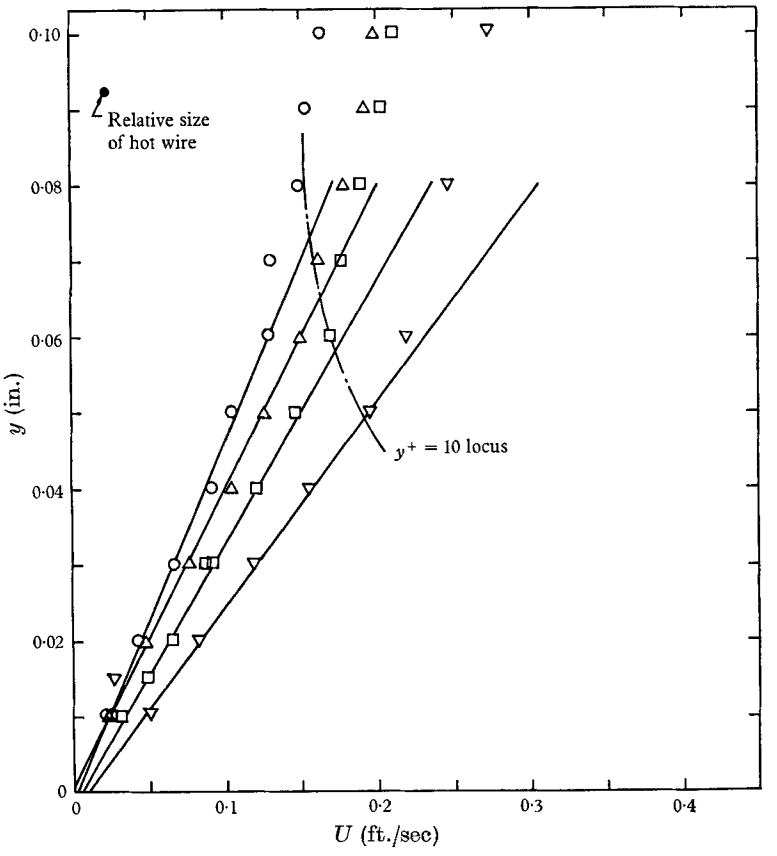


FIGURE 5*a*. Determination of the wall shear stress by the wall-slope method. ▽, station 6; □, station 8; △, station 11; ○, station 15; $dP/dx < 0$.

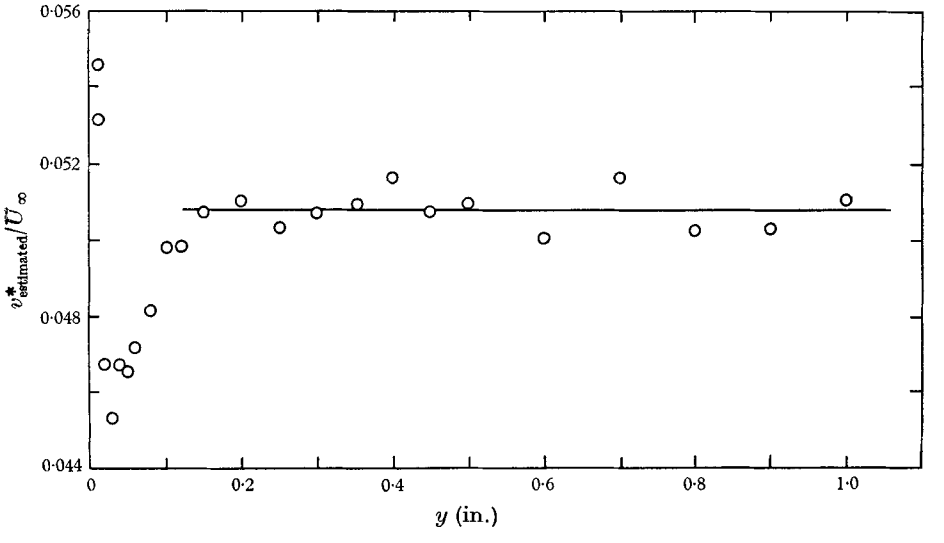


FIGURE 5*b*. Determination of the wall shear stress by the cross-plot method. Station 6, $dP/dx < 0$. $v^*/U_\infty = 0{\cdot}0508$, $U_\infty = 0{\cdot}462$ ft./sec; $v^* = 0{\cdot}023$ ft./sec.

the range 5 in. $\leqslant z \leqslant$ 8 in. was quite two-dimensional in all cases. The data reported here were taken in the middle of this range.

The relatively thick boundary layer made it possible to obtain mean velocity data very close to the wall, which in turn allowed direct measurement of the wall shear stress. Typical surveys in a favourable pressure gradient, where the sublayer is thinnest, are shown in figure 5*a*. The line $y^+ = 10$ is shown for reference. Previous measurements by Laufer (1954) suggest that the velocity profile should be linear from the wall out to at least $y^+ = 5$, where $y^+ = yu_\tau/\nu$, $u_\tau$ is the shear velocity $(\tau_w/\rho)^{\frac{1}{2}}$, and $\nu$ the kinematic viscosity. Since we were able to obtain several points within this region, relatively accurate values of the wall shear stress $\tau_w$ could be obtained from the slope of the mean velocity profile near the wall. The wall-slope method provided one means for determining the shear velocity, and we shall henceforth denote the value so determined by $u_\tau$.

A second method for evaluation of the shear velocity was also employed. This involves fitting the velocity profile in the logarithmic portion of the profile to the 'universal' velocity profile. We chose Clauser's (1956) equation,

$$\hat{u}^+ = 2{\cdot}44 \ln y^+ + 4{\cdot}9, \tag{2.1}$$

where $\hat{u}^+ = U/v^*$, $\hat{y}^+ = yv^*/\nu$ and $v^*$ is the shear velocity. Note that we distinguish between $u_\tau$, the shear velocity determined from the wall-slope method, and $v^*$, the shear velocity determined by fitting the data to Clauser's form of the log law. Our method represents a slight modification of Clauser's; we first observe that

$$yU/\nu = \hat{u}^+\hat{y}^+ = f(U/v^*), \tag{2.2}$$

where the function $f$ can be determined from (2.1). At each point near the wall we calculate $yU/\nu$, and then use (2.2) to establish the local value of $U/v^*$. This is then divided into $U/U_\infty$, yielding an estimate of $v^*/U_\infty$. These values are plotted *vs.* $y$, and yield a constant value in the log region, from which $v^*$ can be determined. This avoids the difficulty of fitting slopes as in Clauser's procedure. Figure 5*b* shows a typical $v^*$ evaluation. The values of shear velocity determined by the cross-plot method ($v^*$) differed somewhat from those determined by the wall-slope method ($u_\tau$); we believe that $u_\tau$ represents the correct wall stress, and that $v^*$ should be viewed as 'that constant which makes our data fit Clauser's form of the log law'. This difference will be discussed again in the next section.

## 3. Experimental results

Five flows were considered in this study. The initial efforts (I) dealt with a turbulent boundary layer in zero pressure gradient. Subsequently two adverse and two favourable pressure gradient flows were examined, and refined mean velocity measurements were obtained in zero pressure gradient.† The free-stream velocity distributions for the four pressure gradient flows are shown in figure 6*a*. Other data are given in table 1. Henceforth the flows will be denoted as follows:

(*a*) $dP/dx \gg 0$ strongly unfavourable pressure gradient,

(*b*) $dP/dx > 0$ mildly unfavourable pressure gradient,

† The later zero pressure gradient measurements were obtained by Liu (1966).

(*c*) $dP/dx = 0$ flat plate pressure gradient,
(*d*) $dP/dx < 0$ mildly favourable pressure gradient,
(*e*) $dP/dx \ll 0$ strongly favourable pressure gradient.

Figure 6*b* shows the variation in

$$K = \frac{\nu}{U_\infty^2}\frac{dU_\infty}{dx} = -\frac{\nu}{\rho U_\infty^3}\frac{dP}{dx},$$

a non-dimensional pressure gradient parameter, for the flows. While there are many dimensionless parameters which can be used to characterize the pressure

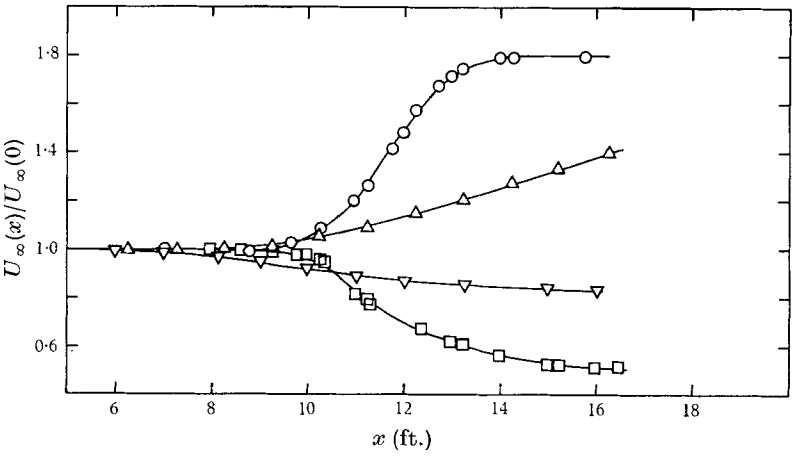


FIGURE 6*a*. Free-stream velocity distributions. ○, $dP/dx \ll 0$; △, $dP/dx < 0$; ▽, $dP/dx > 0$; □, $dP/dx \gg 0$.

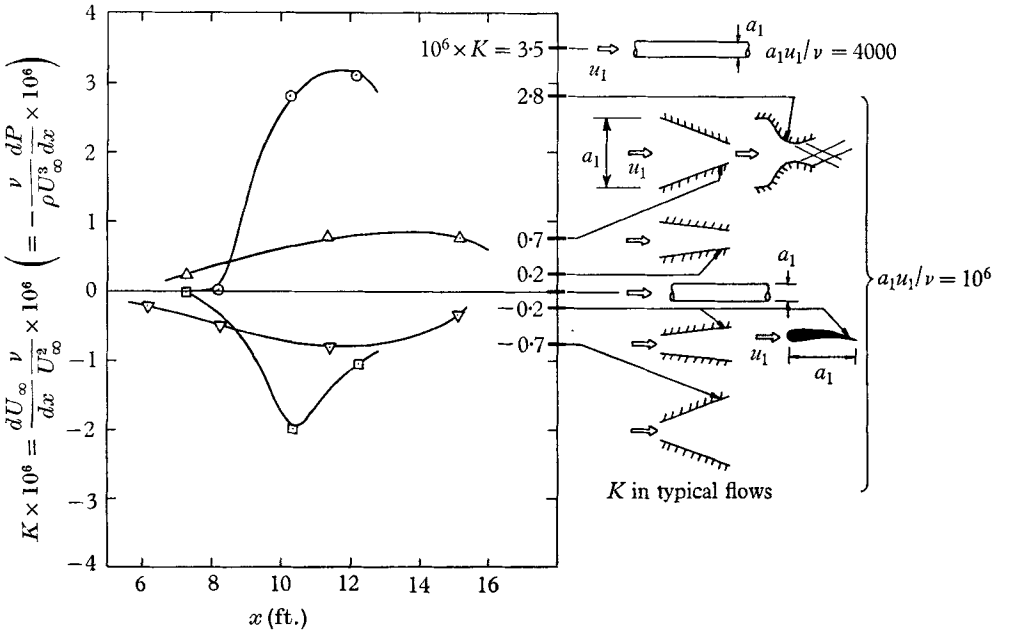


FIGURE 6*b*. Pressure gradient parameter distributions. ⊙, $dP/dx \ll 0$; △, $dP/dx < 0$; ▽, $dP/dx > 0$; ⊡, $dP/dx \gg 0$.

gradient, $K$ is simple to measure, and appears to be physically relevant, as will be discussed later. For comparison, values of $K$ for a few typical flows of practical interest are shown. It should be noted that the pressure gradients imposed on the boundary layers (*a*) and (*e*) are considerably stronger than in most external flow applications, but are quite typical of many internal flow situations.

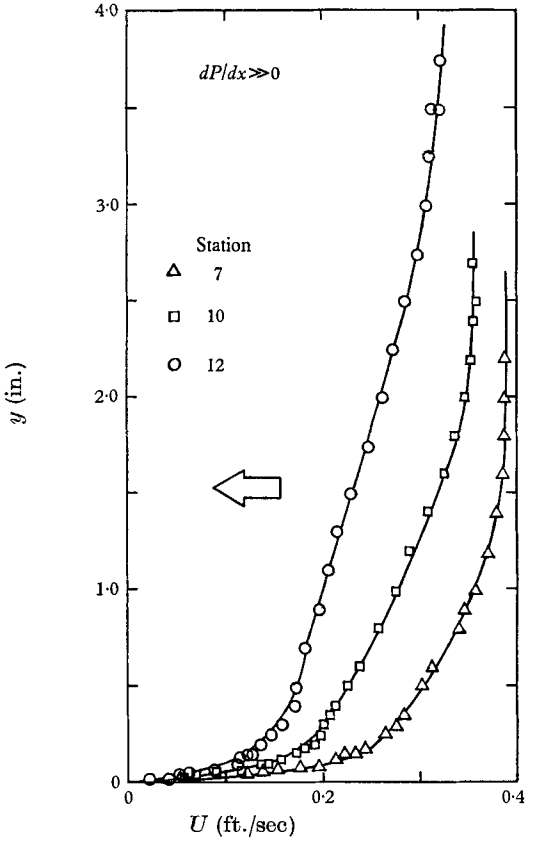


FIGURE 7*a*. Mean profiles for the strong positive pressure gradient flow.

Mean velocity measurements at several stations in each of the five flows are shown in figure 7.† Shear stress data ($u_\tau$ and $v^*$) are included in table 1. The profile data are plotted in the usual velocity defect manner in figure 8. The strongly favourable flow has been omitted because it seemed to undergo relaminarization, and hence should not really be considered or plotted as a turbulent boundary layer. Note that the flat plate is in excellent agreement with the corresponding profile of Clauser (1956). The other three flows shown in figure 8 do not exhibit sufficient similarity that they could be considered as equilbrium layers in the sense of Clauser, although the mild pressure gradient flows are noticeably nearer to equilibrium conditions than are the strong pressure gradient flows.‡

† Note the displacement of the origins for figures 7*b* and 7*c*.

‡ Non-equilibrium flows were purposely chosen for the $dP/dx \neq 0$ tests so that correlation parameters obtained, if any, would not be of a restricted nature.

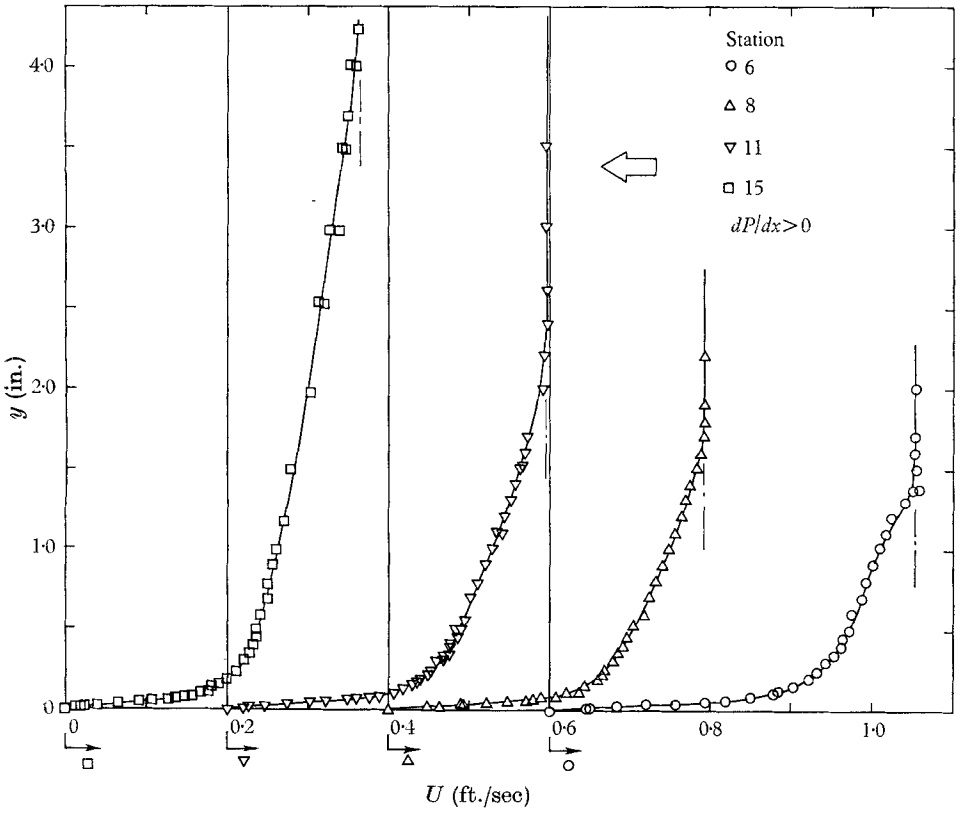


FIGURE 7*b*. Mean profiles for the mild positive pressure gradient flow.

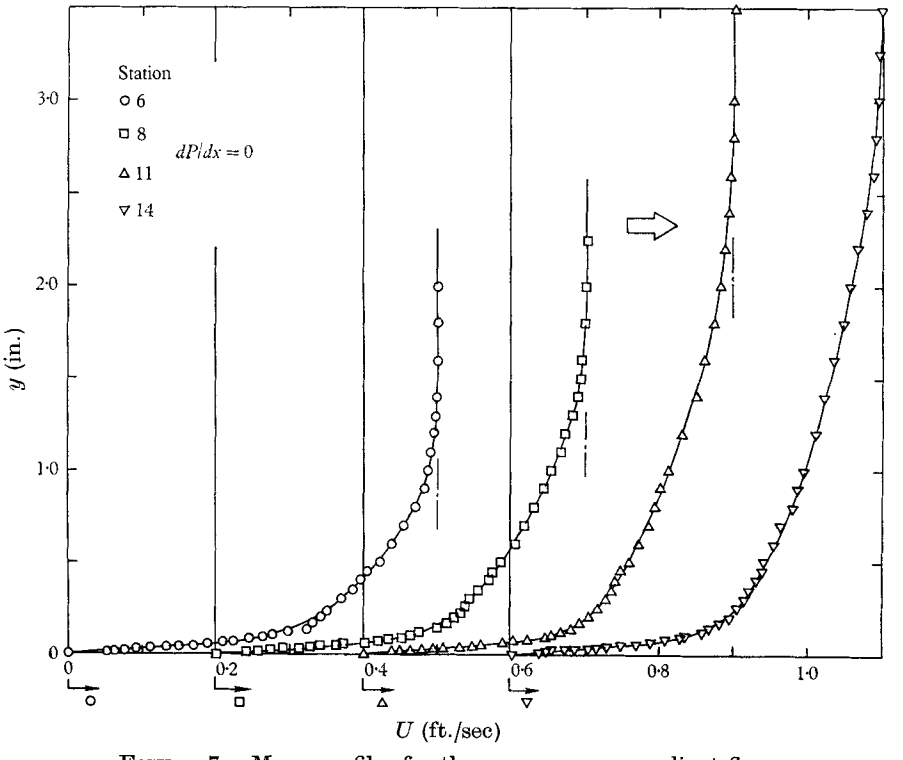


FIGURE 7*c*. Mean profiles for the zero pressure gradient flow.

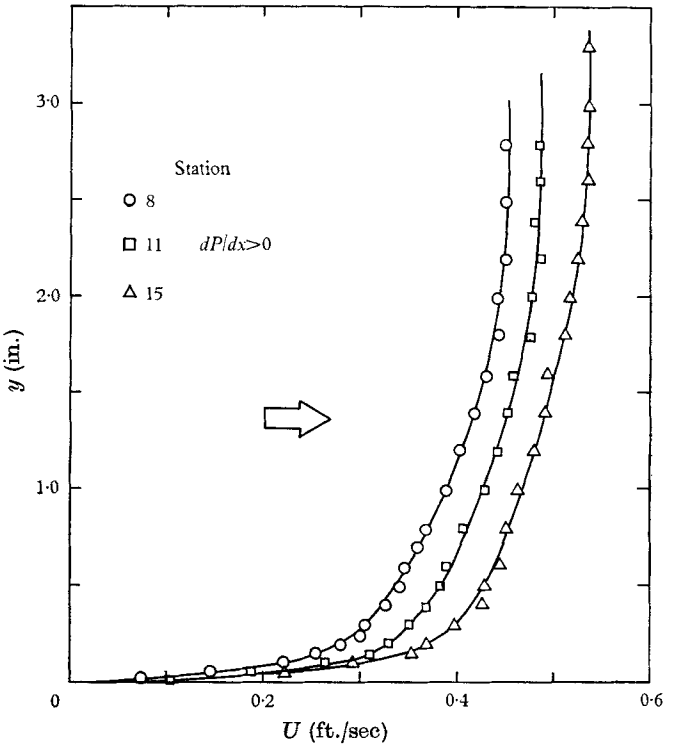


FIGURE 7*d*. Mean profiles for the mild negative pressure gradient flow.

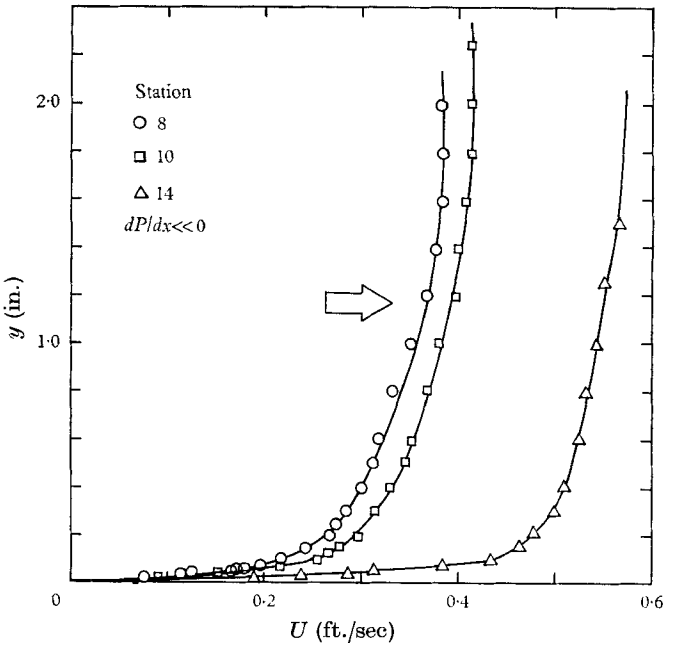


FIGURE 7*e*. Mean profiles for the strong negative pressure gradient flow.

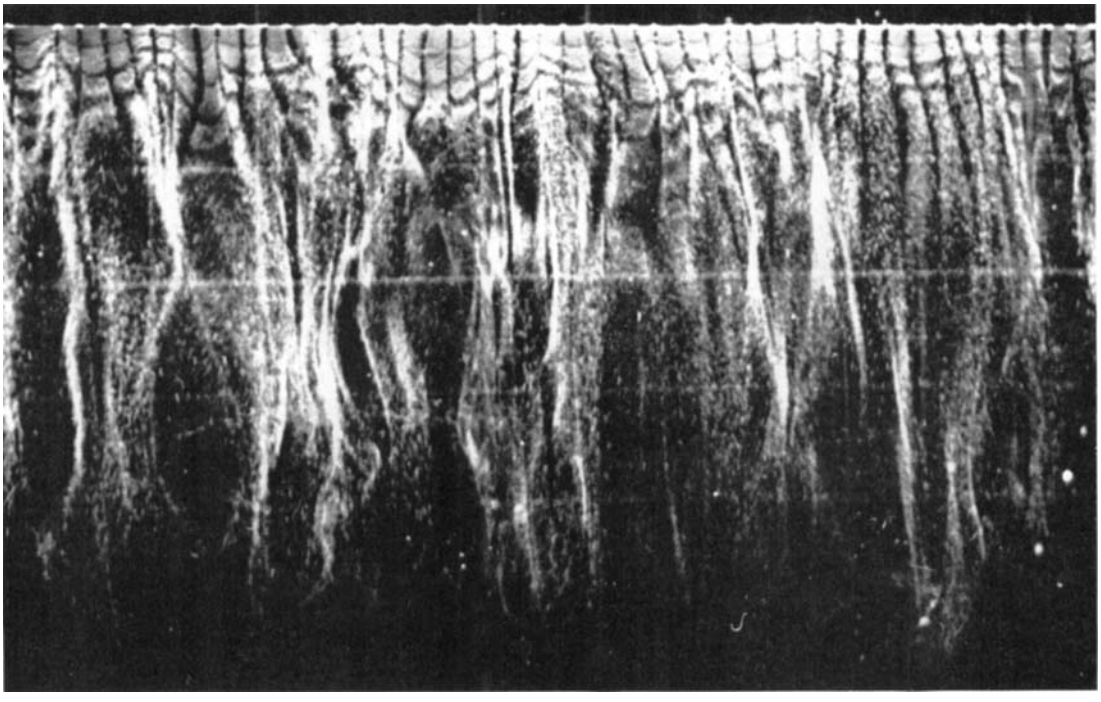

FIGURE 10*a*. $y^+ = 2{\cdot}7$.

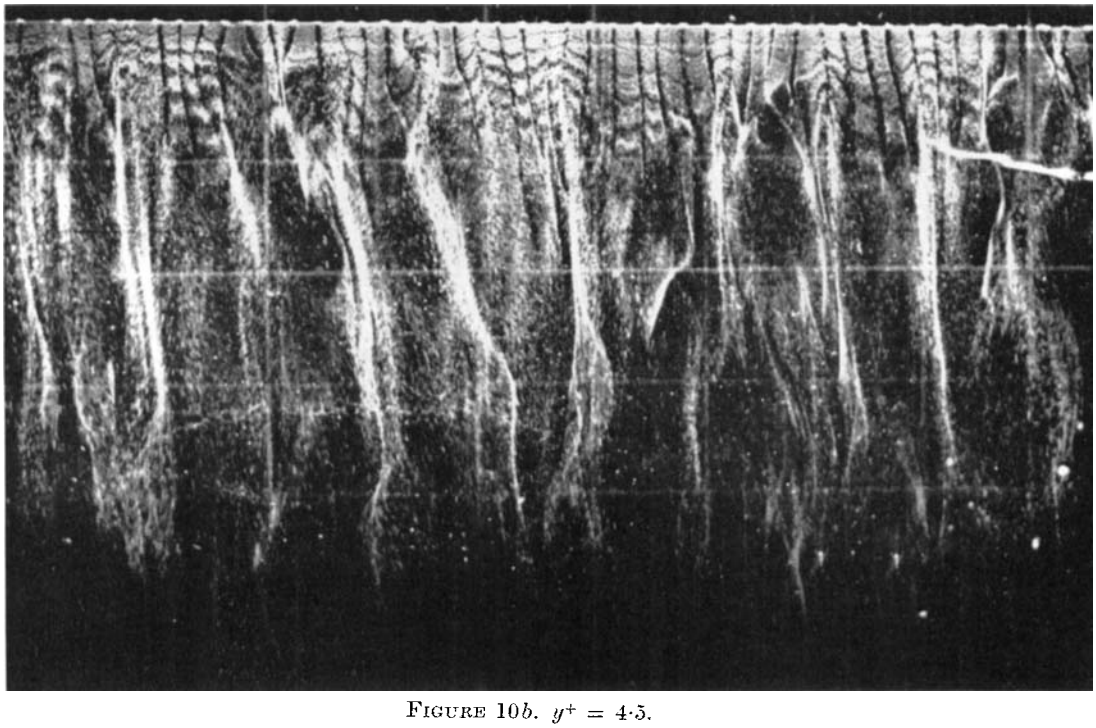

FIGURE 10*b*. $y^+ = 4{\cdot}5$.

FIGURE 10. Photographs of the structure of a flat plate turbulent boundary layer.

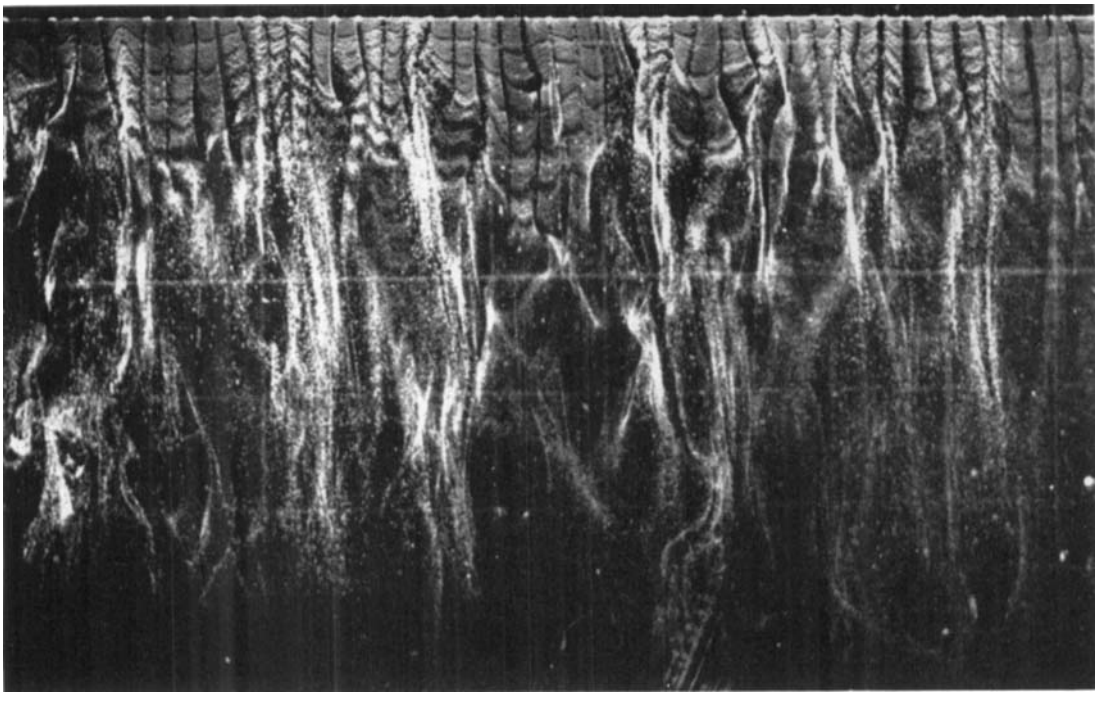

FIGURE 10*c*. $y^+ = 9{\cdot}6$.

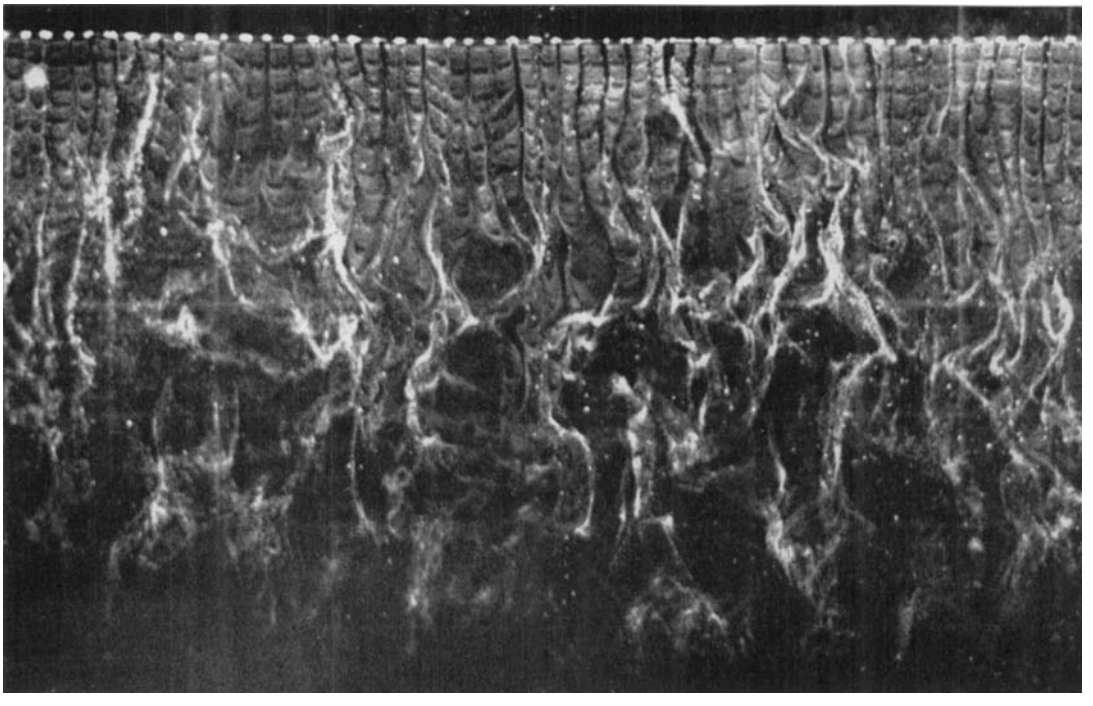

FIGURE 10*d*. $y^+ = 38$.

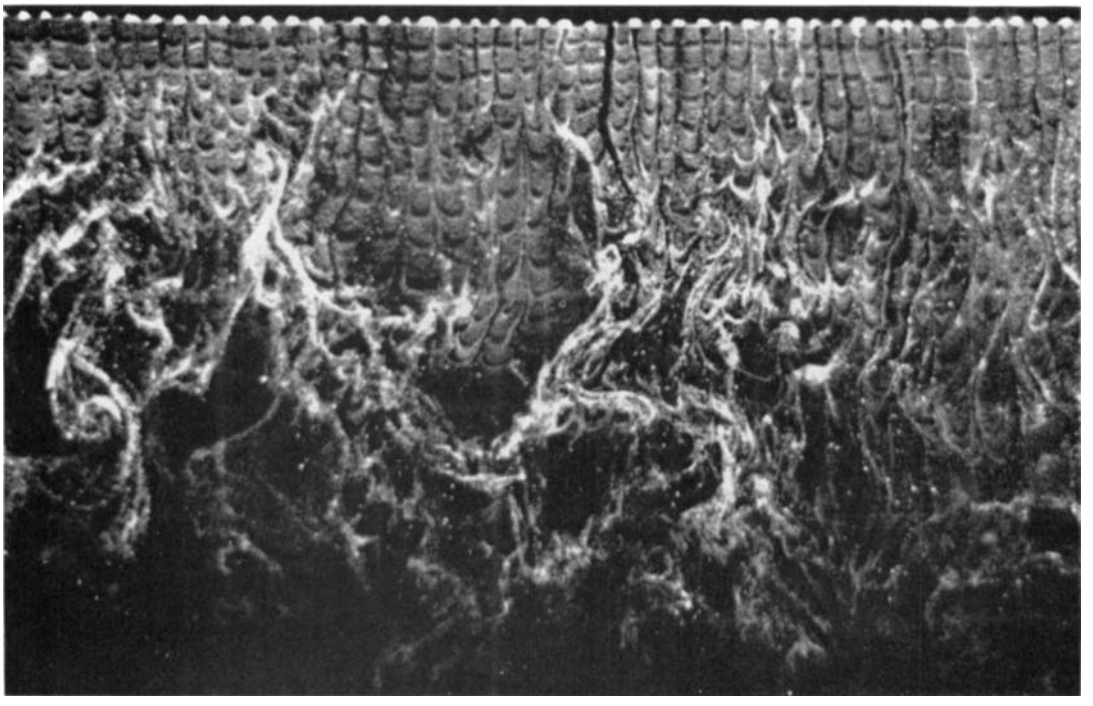

FIGURE 10*e*. $y^+ = 82$.

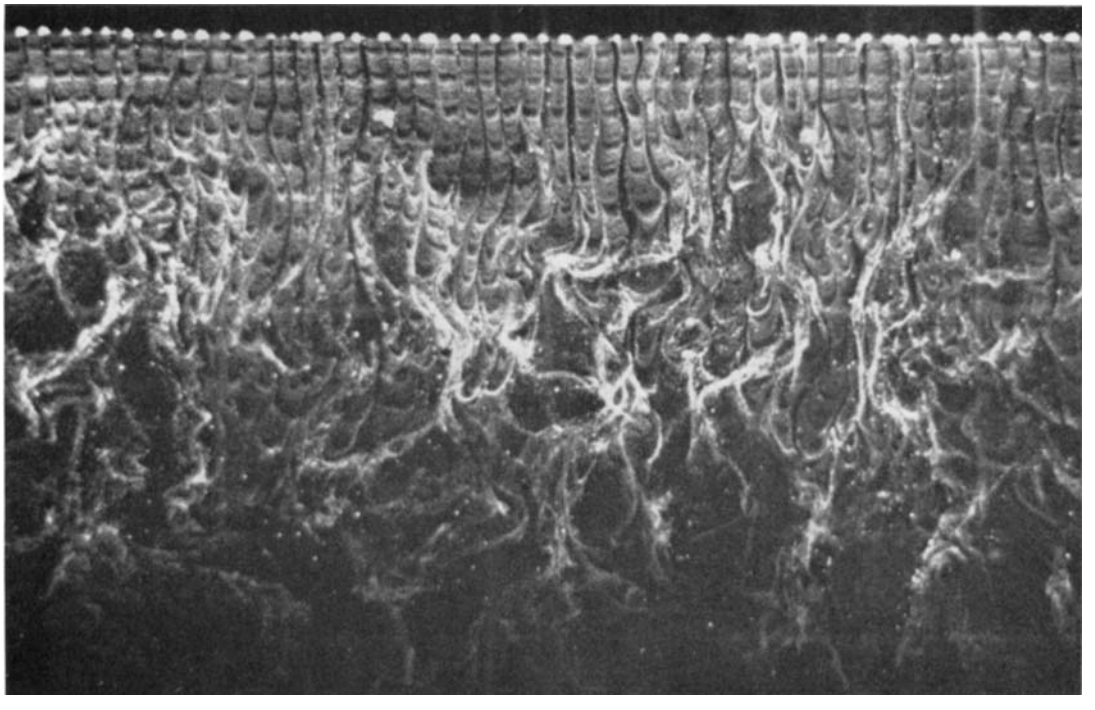

FIGURE 10*f*. $y^+ = 101$.

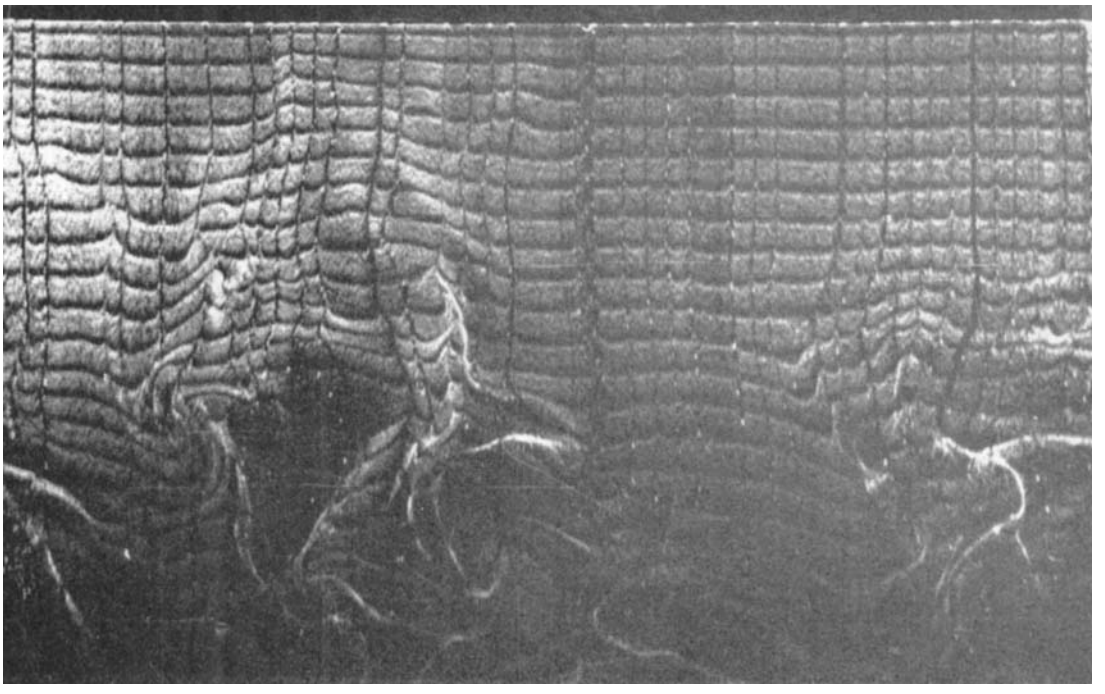

FIGURE 10*g*. $y^+ = 407$.

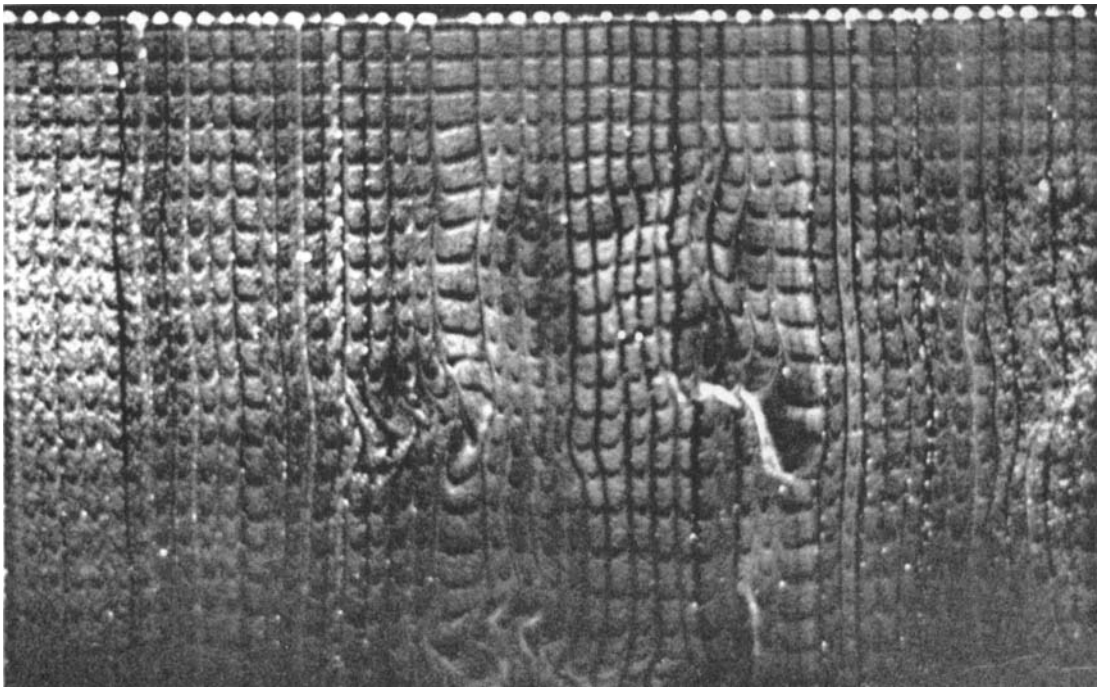

FIGURE 10*h*. $y^+ = 507$.

The mean velocity data are shown in the conventional wall-region form in figure 9. Note that figure 9*a* employs $v^*$, the shear velocity determined by the cross-plot method,† and hence each profile fits (2.1) over a portion of its extent. Noticeable spread of the data in the region $y^+ < 30$ occurs in these co-ordinates. In figure 9*b* we show the same data normalized with $u_\tau$, the shear velocity obtained by the wall-slope method. This collapses the data in the region $y^+ < 30$,

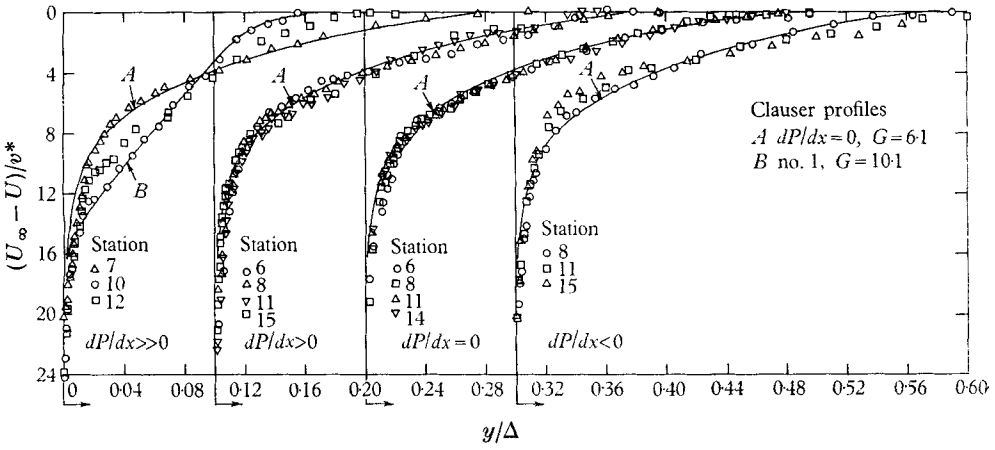


FIGURE 8. Velocity defect profiles.

but spreads it out in the log region. However, comparison of the data for flat plate flow plotted in this manner with the data of Laufer (1951) for channel flow shows excellent agreement. Moreover, Laufer used the wall-slope method, substantiated by channel pressure-drop measurements, and hence his data represent some of the best available in the 'law of the wall' region. Upon examination of the data employed by Clauser in arriving at (2.1), we found that Laufer's (1954) pipe data were employed, but only out from $yu_\tau/\nu = 70$; Clauser's decision on the constants in (2.1) was apparently based on data in which the wall shear stress was not measured directly. Had Clauser instead arrived at an equation which fitted Laufer's channel data, the cross-plot method and the wall-slope method would give the same values for $u_\tau$ and $v^*$, at least for the flat plate flow. More recently Comte-Bellot (1963) showed that the coefficients in the log law depend on the local Reynolds number. These facts suggest that while the cross-plot method does provide a useful parameter for comparison with the defect data of Clauser, the wall-slope method gives more accurate shear stresses, and hence figure 9*b* is taken as our best representation in the law-of-the-wall co-ordinates.

This completes the measurements dealing with the mean velocity profiles, and we now turn to the information obtained visually.

Figure 10, plates 1 to 4, shows the structure of the flat plate turbulent boundary layer as visualized with the hydrogen bubble technique. In these pictures the wire is located parallel to the plate and normal to the direction of flow; the flow is from top to bottom of the pictures. The position of the wire on the $y^+ = yu_\tau/\nu$

† The distinction between $u_\tau$ and $v^*$ is probably essential to correlation of data for general turbulent boundary-layer flows.

| Flow | $x$ (ft.) | $U_\infty$ (ft./sec) | $\delta$ (in.) | $\delta^*$ (in.) | $\theta$ (in.) | $\nu \times 10^6$ (ft.$^2$/sec) | $u_\tau$ (ft./sec) | $v^*$ (ft./sec) | $Re_\theta$ | $H = \frac{\delta^*}{\theta}$ |
|---|---|---|---|---|---|---|---|---|---|---|
| $\frac{dP}{dx} = 0$ | 6·25 | 0·50 | 1·2 | 0·200 | 0·136 | 10·4 | 0·0219 | 0·0247 | 545 | 1·47 |
| | 6·3 (1, 2) | 0·50 | 1·6 | 0·337 | 0·233 | 9·6 | 0·0215 | 0·0233 | 1000 | 1·45 |
| | 8·25 | 0·50 | 1·7 | 0·284 | 0·194 | 10·3 | 0·0214 | 0·0234 | 780 | 1·46 |
| | 10·3 (1, 2) | 0·50 | 2·25 | 0·362 | 0·263 | 10·1 | 0·0212 | 0·0231 | 1080 | 1·43 |
| | 11·0 | 0·50 | 2·6 | 0·420 | 0·293 | 10·3 | 0·0205 | 0·0222 | 1180 | 1·43 |
| | 13·5 (1, 2) | 0·50 | 2·75 | 0·442 | 0·320 | 9·6 | 0·0210 | 0·0228 | 1325 | 1·38 |
| | 14·0 | 0·50 | 3·1 | 0·500 | 0·347 | 10·3 | 0·0192 | 0·0216 | 1400 | 1·44 |
| $\frac{dP}{dx} < 0$ | 8·33 | 0·45 | 2·05 | 0·362 | 0·242 | 10·3 | 0·0202 | 0·0215 | 885 | 1·50 |
| | 11·33 | 0·49 | 2·17 | 0·362 | 0·224 | 9·9 | 0·0204 | 0·0237 | 920 | 1·46 |
| | 15·33 | 0·54 | 2·42 | 0·346 | 0·246 | 9·5 | 0·0217 | 0·0264 | 1160 | 1·48 |
| $\frac{dP}{dx} \ll 0$ | 8·14 | 0·38 | 1·48 | 0·259 | 0·176 | 9·5 | 0·0209 | 0·0198 | 586 | 1·47 |
| | 9·0 (3) | — | — | — | — | 9·5 | 0·023 | — | — | — |
| | 10·25 | 0·41 | 1·60 | 0·252 | 0·171 | 9·5 | 0·0268 | 0·0216 | 615 | 1·47 |
| | 11·0 (3) | — | — | — | — | 9·5 | 0·028 | — | — | — |
| | 12·18 | 0·57 | 1·60 | 0·159 | 0·115 | 9·6 | 0·040 | 0·033 | 567 | 1·35 |
| | 13·5 (3) | — | — | — | — | 9·6 | 0·042 | — | — | — |
| $\frac{dP}{dx} > 0$ | 6·15 | 0·44 | 1·38 | 0·248 | 0·172 | 11·3 | 0·0195 | 0·0223 | 556 | 1·44 |
| | 8·25 | 0·43 | 1·58 | 0·294 | 0·201 | 12·2 | 0·0188 | 0·0205 | 590 | 1·46 |
| | 11·24 | 0·40 | 2·20 | 0·398 | 0·264 | 11·3 | 0·0168 | 0·0185 | 778 | 1·50 |
| | 15·24 | 0·36 | 4·20 | 0·798 | 0·542 | 9·7 | 0·0154 | 0·0157 | 1680 | 1·47 |
| $\frac{dP}{dx} \gg 0$ | 7·25 | 0·39 | 1·53 | 0·287 | 0·173 | 9·6 | 0·0167 | 0·0193 | 588 | 1·65 |
| | 10·15 | 0·36 | 2·30 | 0·518 | 0·319 | 10·0 | 0·0148 | 0·0150 | 957 | 1·63 |
| | 12·23 | 0·32 | 3·40 | 0·898 | 0·540 | 9·3 | 0·0124 | 0·0120 | 1560 | 1·66 |
| $\frac{dP}{dx} = 0$ (2, 4) | 19·0 | 0·197 | — | — | — | 10·4 | 0·0083 | 0·0092 | — | — |
| | 19·0 | 0·434 | 5·00 | 0·697 | 0·505 | 9·8 | 0·0166 | 0·0185 | 2060 | 1·38 |
| | 19·0 | 0·750 | — | — | — | 10·0 | 0·0267 | 0·0296 | — | — |

| Flow | $c_f \times 10^3$ (based on $u_\tau$) | $K \times 10^6$ | $\lambda_v$ (in.) | $\lambda_s$ (in.) | $\lambda_v^+$ | $\lambda_s^+$ | $F$ l/sec-in. | $F^+ \times 10^6$ | $F^+\lambda_v^+ \times 10^4$ |
|---|---|---|---|---|---|---|---|---|---|
| $\frac{dP}{dx} = 0$ | 3·85 | 0·00 | — | — | — | — | — | — | — |
| | 3·7 | 0·00 | — | — | — | — | 1·0 | 123 | — |
| | 3·66 | 0·00 | — | — | — | — | — | — | — |
| | 3·6 | 0·00 | 0·52 | 0·75 | 91 | 131 | 0·99 | 127 | 116 |
| | 3·36 | 0·00 | — | — | — | — | — | — | — |
| | 3·5 | 0·00 | 0·58 | 0·76 | 106 | 136 | 0·98 | 116 | 123 |
| | 2·95 | 0·00 | — | — | — | — | — | — | — |
| $\frac{dP}{dx} < 0$ | 4·04 | 0·21 | 0·73 | 0·85 | 119 | 138 | 0·66 | 112 | 131 |
| | 3·48 | 0·79 | 0·70 | 0·76 | 120 | 131 | 0·71 | 98 | 117 |
| | 3·24 | 0·75 | 0·64 | 0·70 | 121 | 133 | 0·96 | 101 | 122 |
| $\frac{dP}{dx} \ll 0$ | 6·05 | 0·00 | — | — | — | — | 1·07 | 127 | — |
| | — | 0·50 | — | — | — | — | 0·86 | 77 | — |
| | 8·53 | 2·75 | 0·79 | 0·95 | 185 | 222 | 0·58 | 33 | 61 |
| | — | 3·85 | — | — | — | — | 0·18 | 8·9 | — |
| | 9·84 | 3·25 | 0·74 | 0·91 | 256 | 312 | 0·19 | 3·2 | 8·2 |
| | — | 0·56 | — | — | — | — | 1·05 | 16 | — |
| $\frac{dP}{dx} > 0$ | 3·93 | −0·25 | 0·65 | 0·58 | 93 | 83 | 1·02 | 210 | 195 |
| | 3·82 | −0·53 | 0·63 | 0·85 | 82 | 110 | 1·04 | 280 | 230 |
| | 3·52 | −0·83 | 0·66 | 0·88 | 98 | 131 | 0·70 | 226 | 222 |
| | 3·66 | −0·36 | 0·83 | 0·75 | 110 | 99 | 0·61 | 188 | 206 |
| $\frac{dP}{dx} \gg 0$ | 3·66 | 0·0 | 0·72 | 0·81 | 104 | 117 | 0·84 | 198 | 206 |
| | 3·38 | −2·00 | 0·89 | 1·25 | 110 | 154 | 0·73 | 270 | 296 |
| | 3·00 | −1·05 | 1·15 | 1·60 | 126 | 177 | 0·57 | 310 | 388 |
| $\frac{dP}{dx} = 0$ (2, 4) | 3·52 | 0·00 | 0·96 | — | 67 | — | 0·0652 | 148 | 99 |
| | 2·96 | 0·00 | 0·47 | — | 67 | — | 0·530 | 135 | 91 |
| | 2·52 | 0·00 | 0·31 | — | 67 | — | 2·48 | 156 | 105 |

*Notes:* (1) These data obtained with hot-film anemometer in a flow with a thicker inlet boundary layer. (2) $u_\tau$ estimated from $v^*$. (3) $u_\tau$ by smoothed data interpolation. (4) Obtained in wide channel using hot-film anemometer; earlier visual counting scheme.

TABLE 1. Basic data and calculated parameters

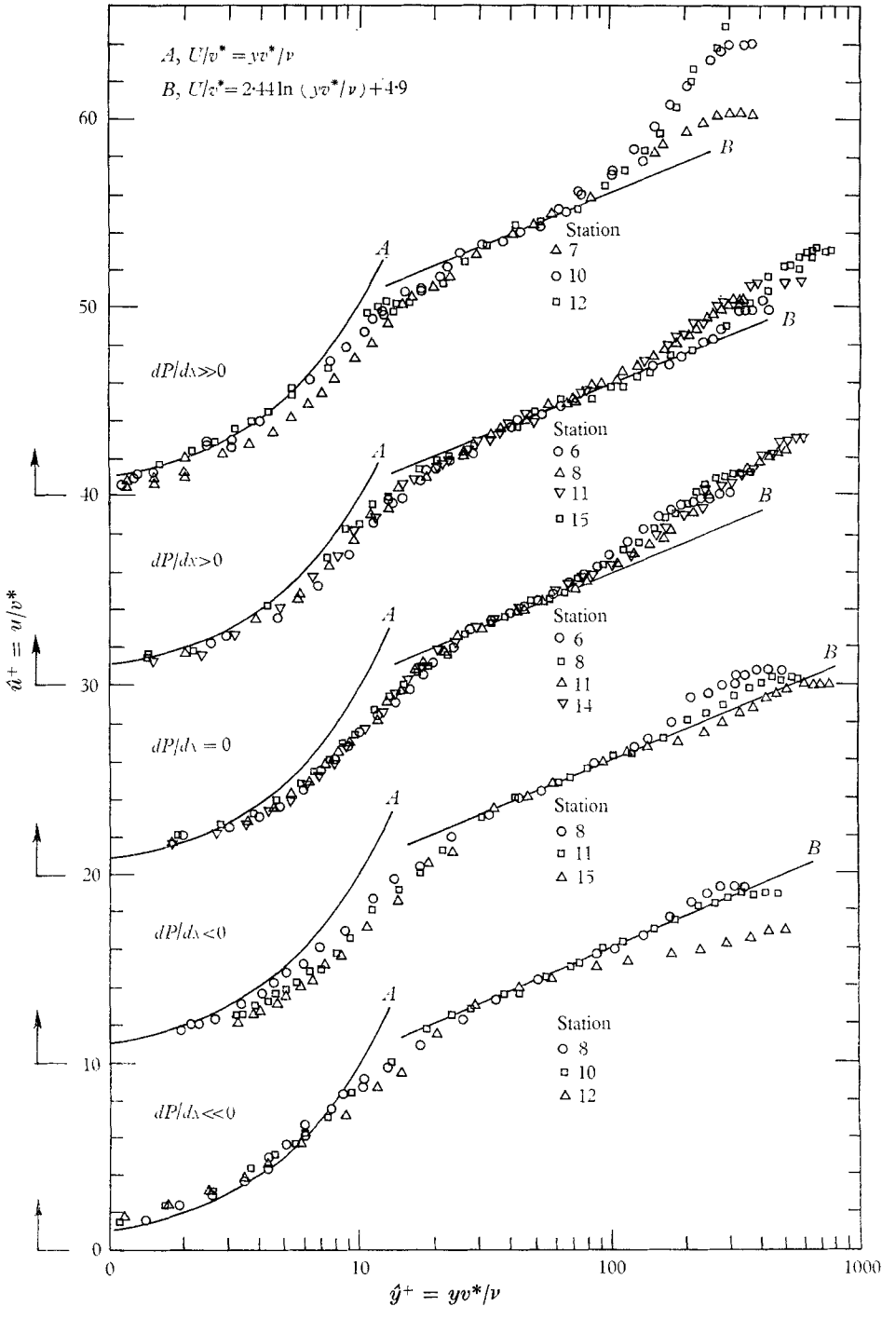


FIGURE 9*a*. $\hat{u}^+$–$\hat{y}^+$ profiles using $v^*$ (note shifted origins).

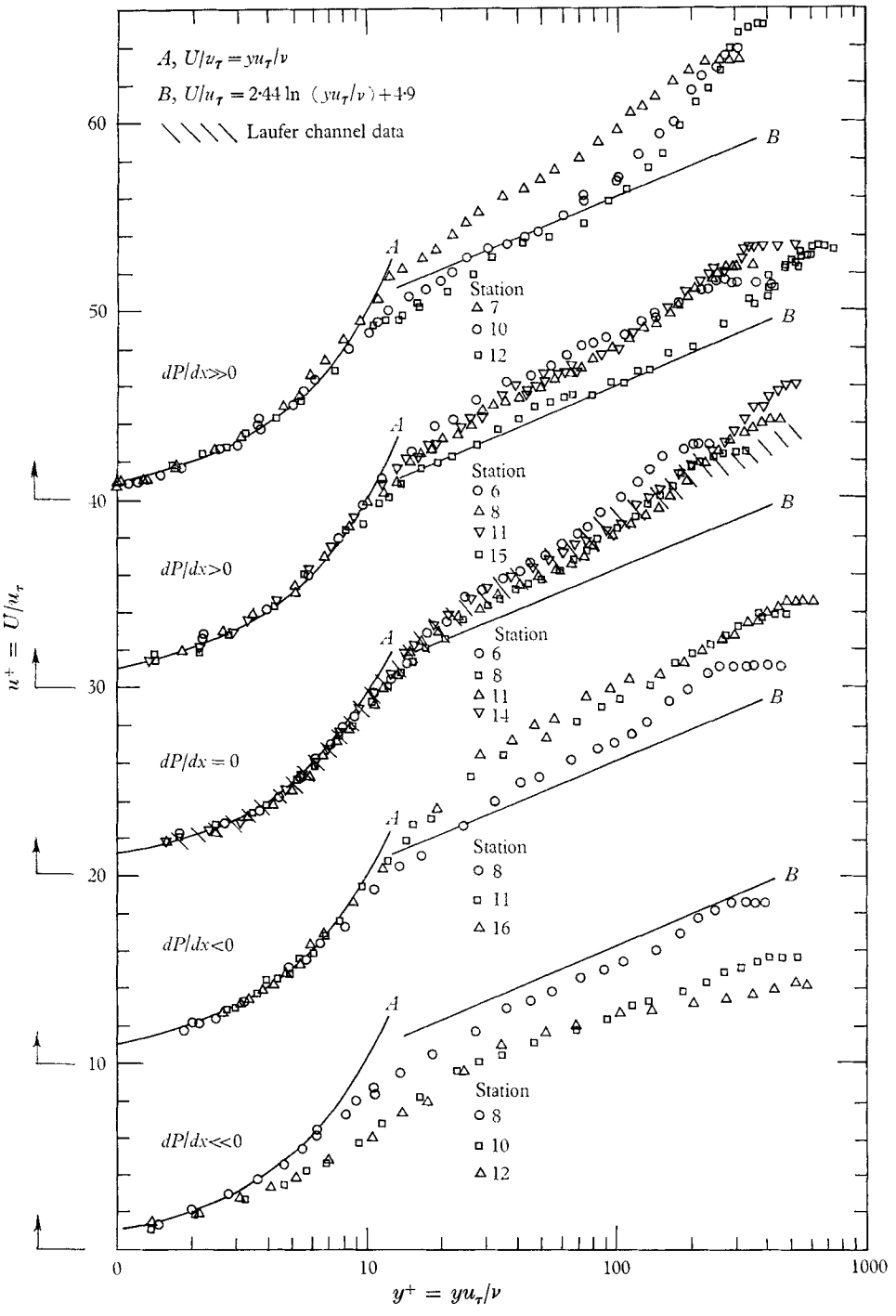


FIGURE 9*b*. $u^+$–$y^+$ profiles using $u_\tau$ (note shifted origins).

scale is shown for each picture. The background reference grid visible in some of the pictures has one inch squares. The time-lines were formed by pulsing the wire voltage; the streaklines were obtained by insulating the wire at about $\frac{1}{4}$ in. intervals along its length. These pictures were obtained with a still camera; corresponding sequences of motion pictures are available.†

Figures 10*a* and *b* show the flow structure in the 'laminar sublayer'. It is clear that, while the flow may indeed be laminar-like in this region, it is both three-dimensional and unsteady. The collection of the bubbles into long streaks by a spanwise component of velocity ($w$) is perhaps the most noticeable feature of this region. Analysis of the still and motion pictures shows that there are very large spanwise variations in the downstream ($u$) component of velocity, and that this variation is apparently correlated strongly with the spanwise velocity. Dye injected through wall slots, or laid on the wall with a hypodermic needle, reveals the same streaky structure with the same mean value of streak-spacing. The streaks, which are regions of low-speed ($u$) fluid, form at rather pronounced spanwise spacings. The streaks waver and oscillate within the sublayer much like a flag, and intermittently seem to leap outwards, sometimes passing rapidly clear to the outer edge of the boundary layer, but more frequently following trajectories within the wall layers. Hence, as we move outwards from the wall (figures 10*c* and *d*), the streaks become less noticeable. The streaks ejected from the wall region become tangled as they enter the outer regions of the flow, making the apparent streamwise and spanwise scales of motion more nearly equal.

Figures 10*e* and *f* show the structure in the 'log' region. Various scales of motion are evident, but there is little evidence of the streaks which are so clearly visible nearer the wall. Note that the entire flow appears to be turbulent. In figures 10*g* and *h* we see the flow in the 'wake' region. The turbulence is clearly intermittent, and of larger scale than in the inner layers. Side views and end views suggest that some of the distortions of the bubble sheets in the wake region are due to their interaction with fluid ejected from the low-speed streaks in the sublayer. When the bubble wire is used well outside of the boundary layer, no distortion of the bubble sheet is visible, indicating that the external flow appears as a quiescent, rectilinear flow when viewed by the same techniques; the small-scale random background fluctuations of the apparatus ($0{\cdot}01 \leqslant \overline{(u'^2)}^{\frac{1}{2}}/U_\infty \leqslant 0{\cdot}02$) do not cause noticeable warping of the marked fluid lines (time-lines) as do the more correlated large-scale motions within the 'turbulent' regions of flow. Turbulent regions are observed out to approximately $1{\cdot}2\delta$, where $\delta$ is the boundary-layer thickness defined by the point where $U = 0{\cdot}99U_\infty$. This visual observation is in accord with hot-wire measurements of Klebanoff (1954).

Systematic visual studies of the flow structure for the five flows (I, II) revealed that the association between the observed structure features and the various regions of the boundary layer is apparently universal for turbulent boundary layers on smooth walls. The size and spacing of the streaks changes from flow to flow, but association of visual and mean velocity régimes appears to be universal. A universal curve of intermittency including photo data, flatness factor

† Engineering Societies Library, 345 East 47th Street, New York, New York, 10017, U.S.A.; request Catalog item R-7, by Runstadler *et al.* (rent or purchase).

data and cut-off data is shown in figure 11 (Liu 1966); it verifies well both the interpretation of the distorted areas of bubble markers as 'turbulent' and the universality of the structure as seen by several observers and types of instruments over a considerable range of Reynolds number.

The streaks tend to be shorter and to wave more violently in adverse pressure gradient flows, and to be drawn longer, and be more quiescent in favourable pressure gradients. In the strongly favourable flow of the present experiments it appeared that the bursting action of the streaks was almost totally suppressed, and the boundary layer showed signs of returning to a laminar state. In contrast, in sufficiently adverse pressure gradients some of the streaks move upstream momentarily, then are washed downstream. This phenomenon is believed to be related to small 'transitory stall' observed in wide-angle diffusers (Moore & Kline 1958), and appears to be a precursor to full stall.

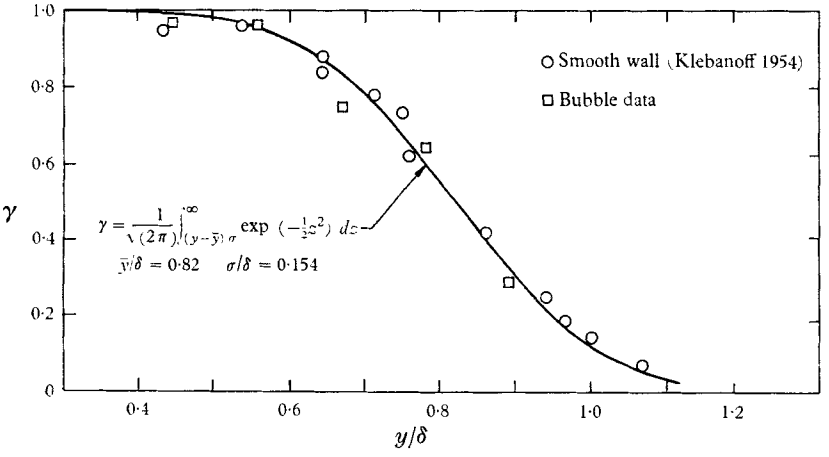


FIGURE 11. Intermittency distribution by the bubble technique.

The streaks are first observed under the Emmons turbulent spots (Meyer & Kline 1961) and in all turbulent regions of the boundary layer downstream. Streaks are not observed using the same techniques in laminar layers. Indeed, in the next-to-last stage of transition (spot growth) one can accurately discriminate laminar from turbulent zones at an instant by observing where streaks occur in the wall layers (Meyer & Kline 1962). The wall-layer streaks are visually distinguishable from the earlier transition streaks reported by Klebanoff, Tidstrom & Sargent (1962) since the wall-layer streaks are much less steady and much narrower.

Much, but not all, of this picture could have been drawn from existing knowledge of the turbulent boundary layer. The new feature is the dominant streaky structure in the sublayer region. These streaks, formed by streamwise vorticity, have been observed as close to the wall as $y^+ = 0{\cdot}15$ with the bubble visualization, and effectively at $y^+ = 0$ with wall-slot dye injection; apparently they persist right to the wall. This suggests the local r.m.s. fluctuation components for $u$ and $w$ approach a constant times the local mean velocity as the wall is approached.

This is not inconsistent with previous measurements (Laufer 1954; Klebanoff 1954).

The streaks were first observed by Kline & Runstadler (1959) during a preliminary survey of the flow structure. The suggestion was then made that the streaks were not only inherent to turbulent boundary layers but also play a very important role in turbulence production near the wall. Subsequently, considerable effort has been expended toward making quantitative measurements of some of the details of the streaky structure and the interaction of the streaks with the outer regions of the flow. These details will next be described.

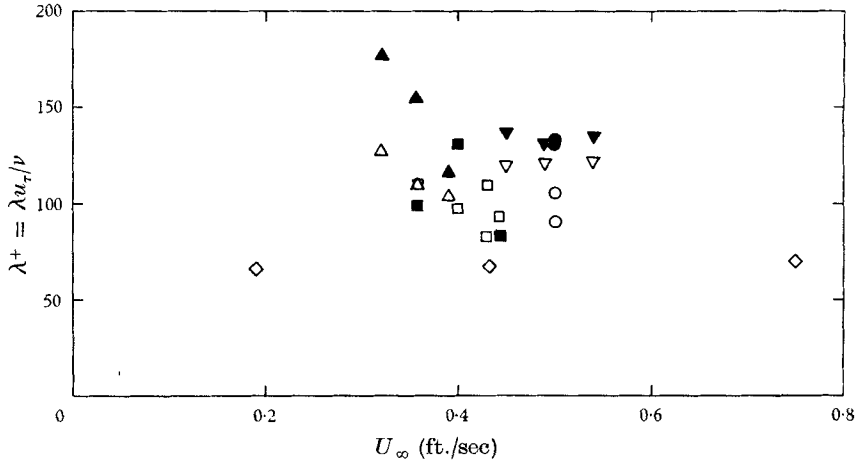


(*a*) $\lambda^+$ as a function of free-stream velocity.

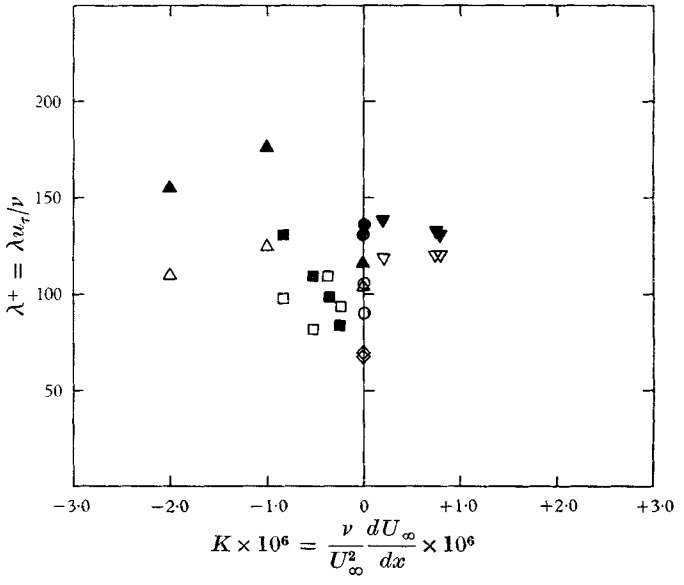


(*b*) $\lambda^+$ as a function of $K$.

FIGURE 12. $\lambda_v$, open symbols; $\lambda_s$, closed symbols; ◇, Runstadler *et al.* (1963) data, $dP/dx = 0$ (old counting scheme); ○, $dP/dx = 0$; △, $dP/dx \gg 0$; □, $dP/dx > 0$; ▽, $dP/dx < 0$.

The average spanwise spacing of the sublayer streaks has been determined visually for the five flows. In (I) the technique involved counting the number of dye streaks for a large number of pictures (50). These counts showed that a reproducible mean spacing exists, though there is considerable variation in the spacing between individual streaks (standard deviation of spacing 30–40 % of mean). In (II) the bubble streaks were counted. While there is certainly some subjectiveness in this procedure, visual counts by different observers were in sufficient agreement as to be clearly meaningful. The data of (II) involved counting very close to the wire; in (I) the counts were made at a fixed distance downstream of the dye slot. This difference probably accounts for some of the discrepancy between the two schemes. Averages over space and time were implicit in both counting schemes.

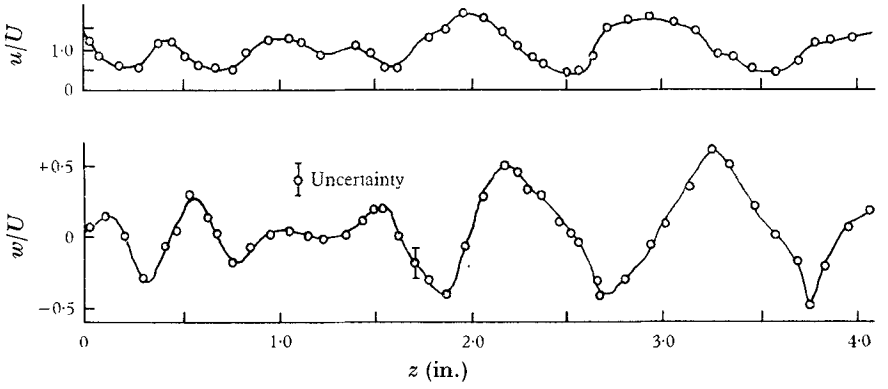


FIGURE 13. Typical instantaneous spanwise variation in $u$ and $w$, determined by the bubble marker method ($y^+ \approx 5$).

The visual counting indicates that the visual mean spacing, $\lambda_v$, correlates on the wall-layer parameters. Figures 12*a* and 12*b* show the value of $\lambda_v^+ = \lambda_v u_\tau/\nu$ as a function of velocity and the pressure gradient parameter $K$ respectively for the four turbulent flows. These data cover a 3 : 1 range in velocities, and a wide range of local pressure gradients. The data indicate that the average (spanwise) streak-spacing corresponds approximately to $\lambda_v^+ = 100$, which is roughly 15 times the thickness of the 'laminar' sublayer. Hence there appears to be a characteristic scale of motion within the wall regions, determined primarily by the wall-region parameters $\nu$ and $u_\tau$.

The hydrogen bubble pictures provide a second more objective method for quantitative determination of the mean streak-spacing. By following the motion of the corners of the time-streak squares, the instantaneous $u$ and $w$ velocity components along the bubble-generating wire can be deduced. Figure 13 is a sample of such data; note that a substantial spanwise region can be surveyed at any instant. The spanwise correlation of the streamwise velocity fluctuation $u'$,

$$R_{11}(0, 0, z_0; 0) = \frac{\int u'(z)\, u'(z+z_0)\, dz}{\int u'(z)^2\, dz},$$

is then computed numerically for each survey. The Fourier transform of this correlation,

$$\hat{U}(l) = 4\int_0^\infty R_{11}\cos\left(2\pi\frac{z_0}{l}\right)dz_0,$$

is then formed using appropriate numerical techniques.† $\hat{U}(l)$ represents the contribution of harmonics of wavelength $l$ to the instantaneous spanwise velocity

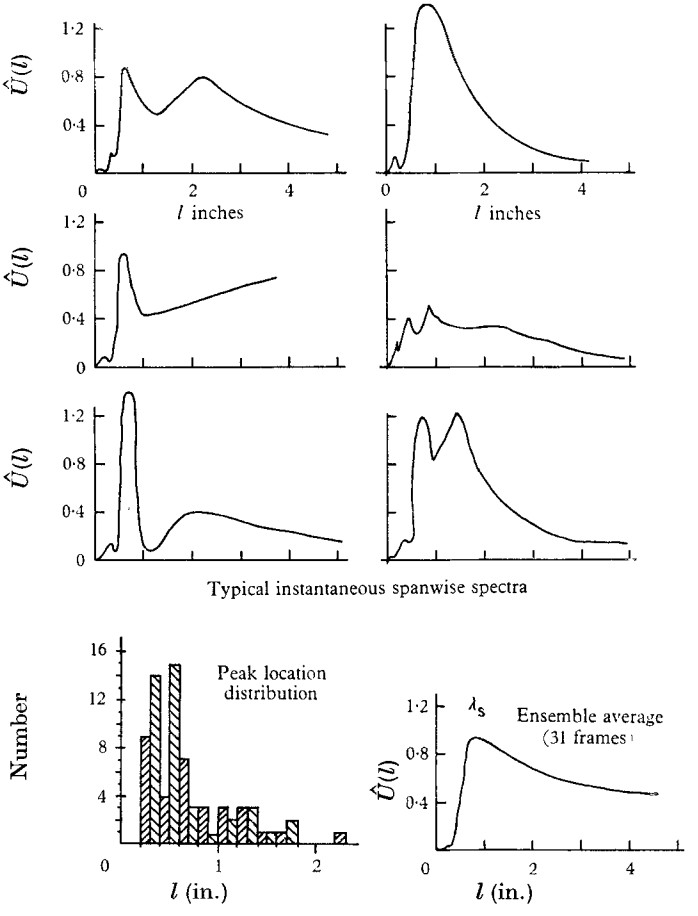


FIGURE 14. Typical instantaneous and average spanwise spectra. $dP/dx \gg 0$, $y^+ \approx 2$.

variation, and hence a peak in the $\hat{U}$ spectrum is expected. Typical samples of such spectra are shown in figure 14. Note that there is considerable variability between individual surveys, but that all display a characteristic peak at roughly the same wavelength. The ensemble average of a large number of surveys becomes stable with a sufficiently large sample, and the location of the peak in this average spectrum can be used to define the average spacing; this spectral definition we denote by $\lambda_s$. The values determined in this more objective manner are shown in figure 12. Note that they are in general greater than those determined

† $R_{11}$ is an even function of $z_0$, hence the cosine transform. An appropriate spectral 'window' was employed (Blackman & Tukey 1959).

by the quicker visual counting scheme (II), but clearly show the same trends as the visual counts. Some of the upward shift appears to be due to the appearance of a harmonic at $\frac{1}{2}\lambda$ not counted in the visual procedure.

The variation in streak-spacing is indicated in the peak distribution histogram (figure 13). This, together with the variability in the individual spectra, indicates that there is no preferred position for the streaks; i.e. they do not arise as a result of some irregularities in the apparatus. This question was also specifically examined, and plots of streak locations for long enough times do show a uniform distribution per unit surface area (II). The same average streak-spacing (determined visually) has been found in three water channels with a number of different active surfaces, providing further evidence that the streaky structure is a result of natural phenomena within the flow.

The peak in the ensemble average spectrum is considerably less pronounced than in the instantaneous spectra. Time-averaged correlations obtained by hot-wire measurements would appear more like the ensemble average, and hence the streakiness probably would not be revealed as clearly as by the (instantaneous) visual studies.†

The second important feature observed in the visual studies is the streak breakup and ejection from the wall. Repeated and careful study of the motion pictures using dye injection shows that these processes occur intermittently and randomly over the surface. Most of the time the streak pattern appears to migrate slowly downstream as a whole, with each streak drifting very slowly outward. Within the innermost layer this motion is smooth and straight, with the streak appearing to become thinner as it moves outward. When the streak has reached a point corresponding to $y^+ \approx 8$–$12$, it begins to oscillate. This oscillation amplifies as it goes outwards and terminates in a very abrupt breakup; most of the breakups appear to occur in the region $10 < y^+ < 30$. After breakup the streak becomes contorted and stretched, and a portion of it migrates outward through the boundary layer along an identifiable 'trajectory'. A sequence of sketches depicting these processes is shown in figure 15. These sketches represent typical side views, as seen in the motion pictures. The arrow follows a prominent portion of the ejected streak. The oscillation is clearly evident in the third sketch, and the contortion in the fourth and fifth.

The motion pictures, particularly more recent side and end views, suggest that the slow streak lift-up is a result of the streamwise vorticity. These secondary motions collect low-speed fluid into streaks, and then lift the streaks gradually away from the wall until a point is reached where some sort of sudden instability appears to occur. The amplifying rapid oscillation we have called 'breakup' then follows. This process seems almost to fling low-speed fluid away from the wall and out into the faster flow. It is the striking violence of this bursting process which suggests that the streak breakup plays a dominant role in the transfer of momentum between the inner and outer regions of the boundary layer.

It is difficult to quantify the breakup process, but some information has been

† Indeed, the 'ensemble' here is still for a limited number of frames (30); there is a question if the streaks will show at all for very long time averages unless filtering is used. See discussion by Kronauer to article by Kline (1965*b*).

obtained by extensive study of the motion pictures. By examining the plan view pictures in which wall slot dye injection was employed, the number of breakups of streaks fed by a certain span of dye slot can be counted for a given time interval. Interpretation of these numbers is not entirely clear. While the counting is confined to a particular field of view, it does not really allow determination of the

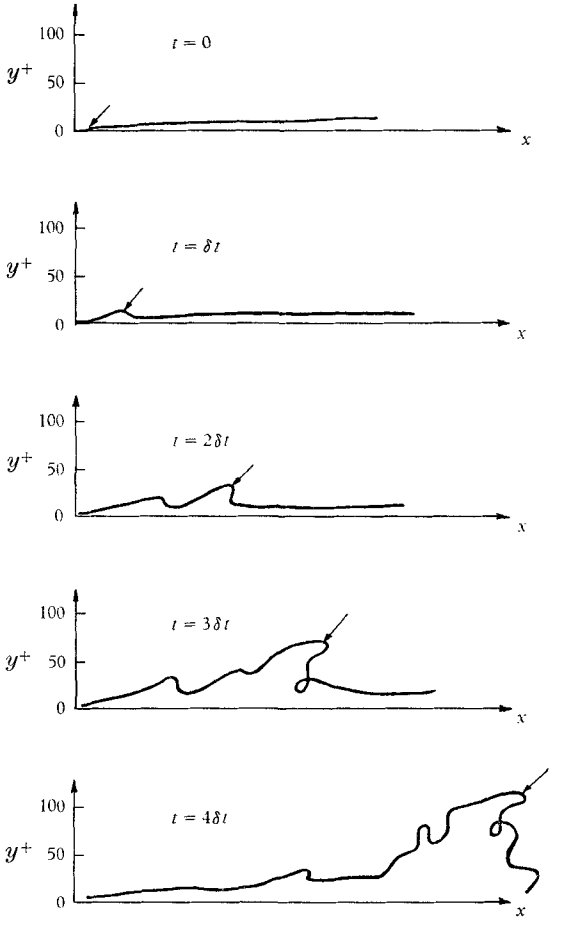


FIGURE 15. Dye streak breakup; illustration as seen in side view.

breakup rate per unit of surface area, since the dye slot only feeds those low-speed regions passing over it. It seems that the best interpretations of the breakup frequency $F$ determined in this manner is as the frequency of streak breakup *per unit of span*. The number $1/(F\lambda)$ might then be interpreted as the average lifetime of a streak.

One might expect to find some correlation of spectral data at a circular frequency $\omega = 2\pi F\lambda$. Black (1966) has indeed found that wall-pressure gradients correlate on the wall-layer parameters at a dimensionless frequency $\omega^+ = \omega\nu/u_\tau^2 = 0{\cdot}056$. This value is also given by his simplified analysis. Our measurements yield $\omega^+ = 2\pi F^+\lambda^+ \approx 0{\cdot}06$ for the flat plate flow;† this remarkable agreement lends

† Note that this value does not hold for $K \neq 0$ (table 1).

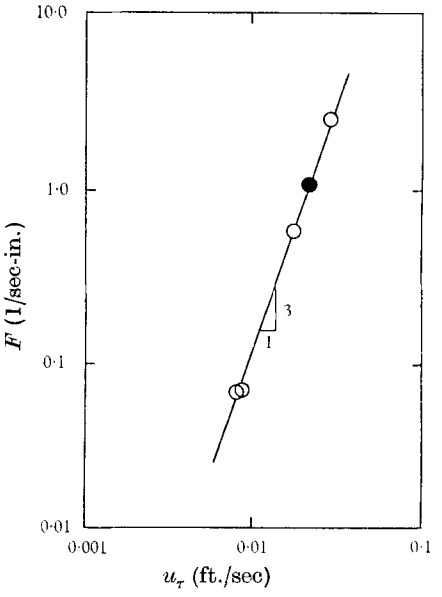


FIGURE 16*a*. Burst rate as a function of shear velocity. $dP/dx = 0$; ○, Runstadler *et al.* (1963), 3 velocities; ●, present data, $3x$ stations.

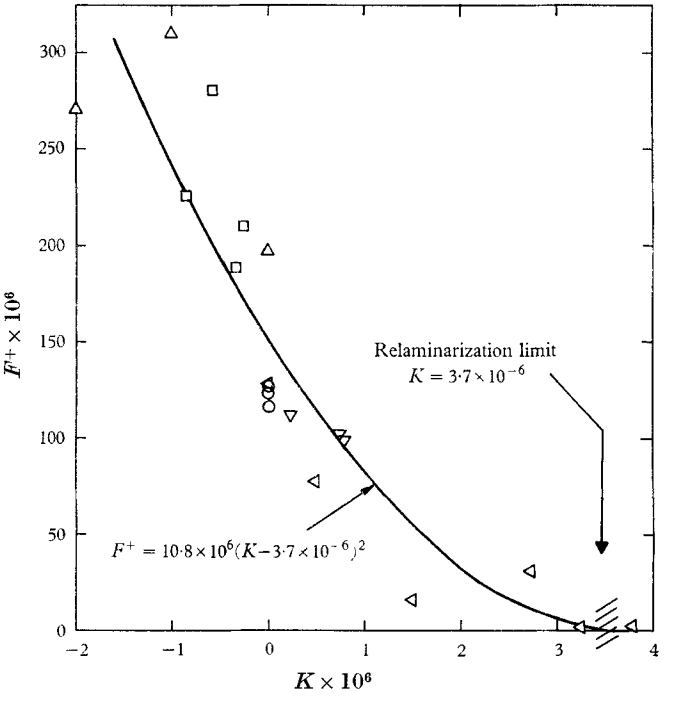


FIGURE 16*b*. Normalized burst rate as a function of $K$. △, $dP/dx > 0$; □, $dP/dx > 0$; ○, $dP/dx = 0$; ▽, $dP/dx < 0$; ◁, $dP/dx \ll 0$.

credence to the notion that there is an inherent breakup frequency for the wall-layer flow.

Assuming that $F$ should be normalized using $\nu$ and $u_\tau$ (with $K$ as a parameter), dimensional analysis suggests that the dimensionless group $F^+ = F\nu^2/u_\tau^3$ should be some function of $K$. The data for the flat plate flow are shown in figure 16*a*,

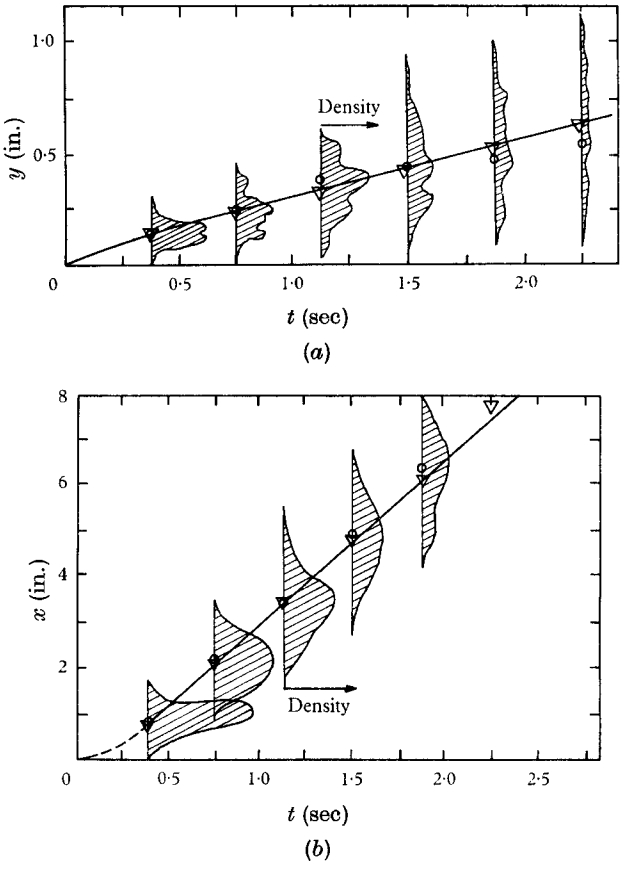


FIGURE 17. Trajectories of ejected eddies—flat plate flow. Station 10, $dP/dx = 0$; $\nabla$, averages; O, maxima.

where $F$ is seen to vary as $u_\tau^3$ for the range of data available. In figure 16*b*, $F^+$ is plotted *vs.* $K$ using the data from the five flows. The important feature is the apparent cessation of bursting when $K$ exceeds about $3{\cdot}7 \times 10^{-6}$. This is essentially the value of $K$ at which Kays & Moretti (1965) observed relaminarization of a turbulent boundary layer in heat transfer experiments with air and Launder (1964) found similar results with a hot wire in air. The good agreement of these data further support the view that the bursting process plays a crucial role in turbulence production and in the interaction between the inner and outer layers.

The trajectories of the ejected eddies can be evaluated quantitatively, and this has been done using side view motion pictures (with dye) from the five flows.

In each case there is quite a variation among individual trajectories, but by considering a large enough sample a stable average can be obtained at any point. Figure 17 shows the distribution and average trajectories for the zero-pressure-gradient case. Note that the average trajectory and the 'most probable' trajectory are essentially the same, though the variance in trajectories is quite substantial. The streamwise velocity component of the dye particle leading the ejected streak outwards has also been determined; figure 18 shows the ratio of the dye filament velocity to the local average velocity as the filament passes outwards through the boundary layer. Note that the flat plate data correlate remarkably well. Further examination of this correlation (II) suggests that beyond

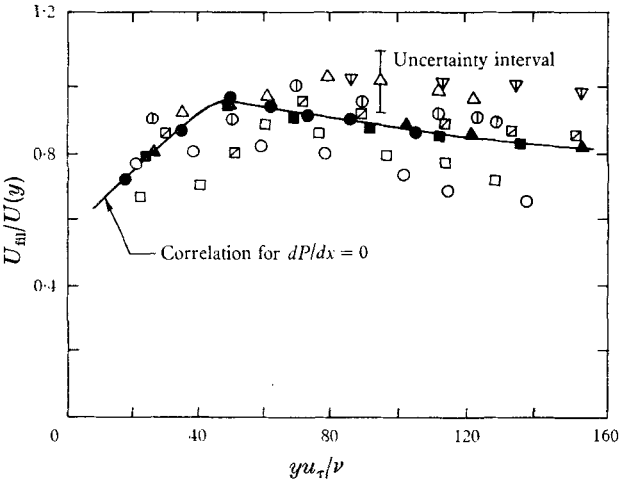


FIGURE 18. Average velocities of ejected eddies.

| $dP/dx < 0$ Station | | $dP/dx \gg 0$ Station | | $dP/dx = 0$ Station | |
|---|---|---|---|---|---|
| ⌀ | 8 | △ | 7 | ● | 6 |
| ⊠ | 11 | ○ | 10 | ▲ | 10 |
| ▽ | 15 | □ | 12 | ■ | 16 |

$y^+ = 40$ the ejected fluid continues to move through the boundary layer at a velocity corresponding to $U_{fil}/u_\tau \approx 13{\cdot}8$, which is essentially the mean velocity at $y^+ = 40$. Hence in a sense the ejected eddies can be viewed as being 'born' in the wall region, and cast out into the log region from a position at the edge of the 'buffer' layer. It is also interesting to note that the ejected fluid moves at something less than the mean velocity, and at roughly 80 % of the mean velocity in the outer part of the boundary layer. This is reminiscent of the observation by Klebanoff (1954) that the turbulent regions in the intermittent portion of the boundary layer move at about 80 % of the free-stream speed; however, no clear evidence is yet available concerning either a relation or a lack of relation between these two observations.

This completes the quantitative information on the flow structure available at this writing. In the following section we give our present 'best interpretation'

of the complicated processes of the turbulent boundary layer, drawing additional insight from further experiments, of a somewhat different nature, now partially completed.

## 4. Discussion

These observations have led us to the conjecture that the wall-layer streak breakup plays an important role in determining the structure of the entire turbulent boundary layer; in particular, we believe it dominates the transfer processes between the inner and outer (wake) regions. In this section we shall first discuss the mechanics of streak formation and breakup, and then discuss related evidence supporting this conjecture.

A plausible physical explanation for the formation of wall-layer streaks was essentially proposed by Lighthill (1963), though not quite in this connexion. Lighthill observed that a natural effect of flow towards and away from a wall is the turning of the flow, as shown in figure 19*a*. This turning action would act to convect and alter the spanwise vorticity component, as shown in the sketch. Vortex lines would be stretched in regions where the flow is towards the wall, and compressed in regions of outflow. Since the spanwise component of vorticity is primarily due to $\partial u/\partial y$, this stretching and compression would lead to spanwise variation in $u$ near the wall. Where the flow is towards the wall, the spanwise component of vorticity would act to increase the local $u$ in the sublayer. Where the flow is outwards, $u$ would be reduced by vortex line compression. Hence a spanwise variation in $u$ can develop naturally as a result of the inherent three-dimensionality of the coexisting turbulence. The streamwise vorticity so generated would collect low-speed fluid near the wall, and when markers are put into the wall layers the streaks would become visible. The same secondary vorticity would account for the lifting of the low-speed wall-layer streaks observed experimentally prior to the breakup process.

A similar and possibly related streaky structure is observed in the middle stages of natural laminar–turbulent transition (Elder 1960). In a series of experiments, Klebanoff *et al.* (1962) examined the formation and properties of these 'transition streaks'.† In some of the experiments, the transition streaks were purposely fixed in location by their apparatus, and were very regular and periodic so that detailed studies were possible. It was found that the $u$ component of velocity was low in the region where the flow was moving away from the wall (Klebanoff's 'peaks'), in accord with the arguments above.

While considerable similarity exists between the transition streaks and the wall-layer streaks, there are important differences in their respective scales, steadiness, and apparently in their requirements for pre-existing fluctuations. The relatively widely spaced transition streaks break down to form propagating turbulent spots, with smaller, more closely spaced wall-layer streaks appearing at the wall under the spots. The transition streaks can be fixed in location by relatively minor effects such as the screeen weaving far upstream (early experiments of Klebanoff *et al.*). On the other hand, the wall-layer streaks are less sensitive to

† In this section we use 'wall-layer streaks' and 'transition streaks' to distinguish the two types clearly.

minor upstream changes, and they move in position in such a way that their distribution over the area is random for long times. The transition streaks grow gradually in a relatively quiescent laminar flow, while the wall-layer streaks have been observed only in response to relatively large amplitude fluctuations.† Nevertheless, the mechanisms for formation of the two types of streaks are probably closely related, and hence the transition studies shed considerable light on the turbulent wall-layer problem.

In examining the mechanisms of wall-layer streak breakup, we again turn to the analogy with the transition streaks. In the controlled transition experiments of Klebanoff *et al.* (1962) and Kovasnay, Komoda & Vasuedva (1962), intense local shear layers (vorticity concentrations) were periodically‡ formed in the outer portion of the transition boundary layer in spanwise positions corresponding to the streaks (the 'peaks'). This appears to be due to vortex stretching at the outer edge of the boundary layer. These local shear layers periodically become locally unstable and break down in violent oscillation,§ reminiscent of the local breakdown processes of the wall-layer streaks in the turbulent boundary layer. Stuart (1965) has made a very simple model of the vortex-stretching processes for the transition problem, and his model displays the important features observed experimentally. The vortex-stretching mechanism is found to be essential to the development of the intense shear layers in these controlled transition experiments; the evidence at hand suggests it is of similar importance in the breakup of wall-layer streaks in a turbulent boundary layer. A picture of this mechanism of breakup is given in figure 19*b*.

The suggestion that vortex stretching leads to the intermittent formation of intense local shear layers, and hence perhaps to a locally unstable breakup, has led us to initiate a study of the instantaneous $u$ velocity profiles normal to the wall. The prime tool in these experiments is a hydrogen bubble generating wire mounted normal to the plate. Preliminary visual studies indeed indicate that the random eddy motions in the outer portions of the flow interact with the low-speed streaks to form momentary regions of concentrated vorticity just outside of the sublayer. Those which persist sufficiently long appear to undergo a rapid breakdown, possibly because of their dynamic instability. While these early results are not yet conclusive, they do already provide further evidence for the notion that randomly formed local shear layers provide a source of dynamic instability, particularly in the region very near the wall.‖ The idea of intermittent breakdown is also consistent with the observation that the higher-frequency components of a hot-wire signal are intermittent (Sandborn 1953).

In any turbulent shear flow turbulence production occurs through the average

† See, for example, the motion pictures of natural transition by Meyer & Kline (1962). These films show that the process of cross-contamination, i.e. spot growth, occurs at the spot edges due to a strong wave-like disturbance. This disturbance creates new wall-layer streaks in fluid that was previously laminar, and the effect is observed only locally where the disturbances are large.

‡ The method of artificial disturbance introduced regular periodicity.

§ The movies of Meyer & Kline (1962) vividly show this effect in natural transition.

‖ A similar idea has been suggested by Betchov & Criminale (1964) as a possible mechanism of importance at the outer edge of the boundary layer.

action of the turbulence Reynolds stress against the mean velocity gradients. In free shear layers, and in the outer regions of turbulent boundary layers, the turbulence consists of weakly correlated (i.e. small $\overline{u'v'}$) motions. The strong

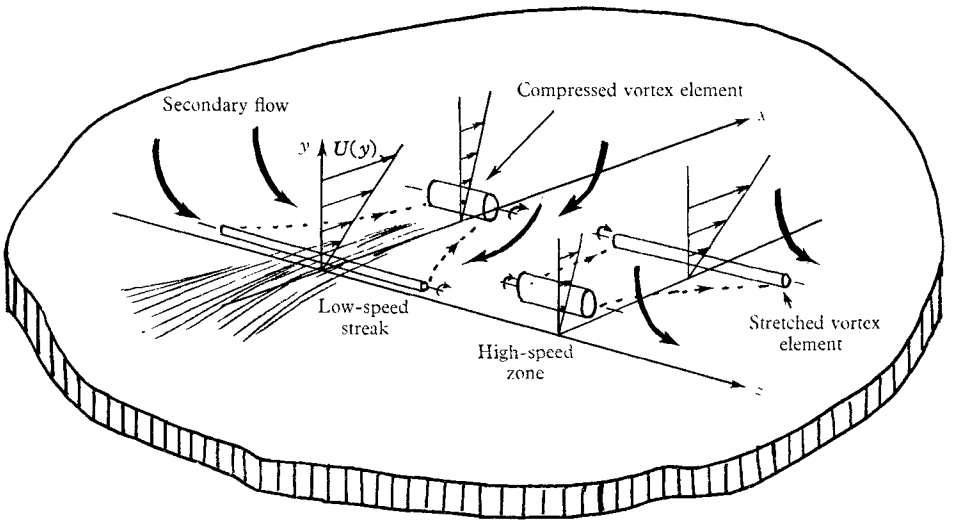


FIGURE 19*a*. The mechanics of streak formation.

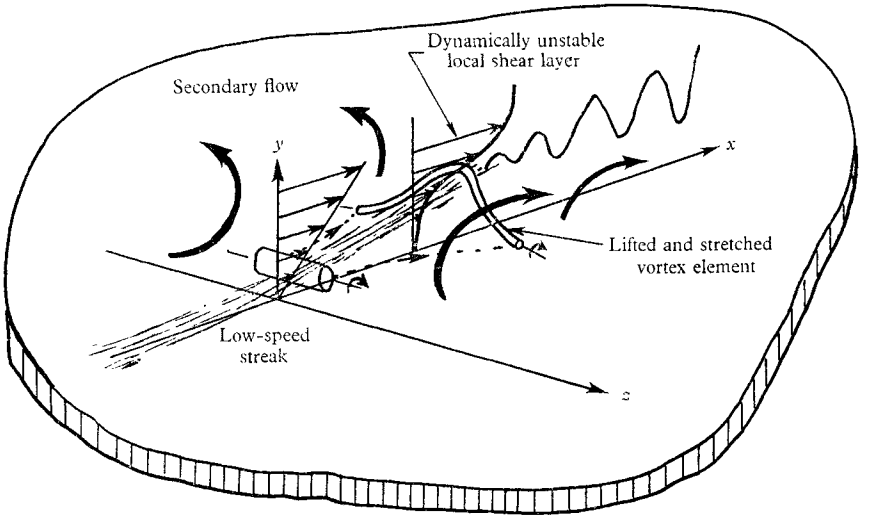


FIGURE 19*b*. The mechanics of streak breakup.

correlation and high Reynolds stress which characterize the wall region of bound shear flows must arise because of some well-correlated motion; we believe the streak breakup provides this organized motion. The Reynolds stress associated with the break up motions is probably greater than that of the background turbulence, and hence breakup may make a substantial contribution to the

turbulence energy production per unit volume particularly in the wall region.† Moreover, the ejection extends this highly correlated motion into the outer flow along the streak trajectory, i.e. over a substantial portion of the entire boundary layer (figure 17). Hence the dominance of the streaks is not confined to the region of their origin or breakup; directly or indirectly they affect most of the flow. A test of these ideas could be obtained by measuring the instantaneous turbulence production rate and correlating this with streak breakup events. Such a study is now in progress.

There is a considerable body of indirect support for the idea that the wall-layer streak formation and breakup play a central role in turbulent boundary-layer processes. The most striking evidence deals with several methods for relaminarization of turbulent flows by suppression of the streak breakup process. The effect of acceleration has already been discussed. Additionally, Cannon (1965) visualized turbulent flow in a rotating tube fed by fully established turbulent pipe flow from a stationary inlet section. He found that turbulent flow can be completely suppressed by rotation at Reynolds numbers as high as 20000 and partially suppressed to 40000 by relatively small amounts of rotation (small Rossby number). An explanation of this phenomenon offered (by S. J. K.) in advance of the experiments was that the centrifugal field induced by rotation would act preferentially to hold the low-speed streaks on the wall; this in turn reduced bursting action. Similarly, relaminarization has been observed on one wall of a two-dimensional channel rotating about an axis located parallel to the wall,‡ while the bursting on the other wall is increased in frequency and intensity. In this case Coriolis forces provide the streak stabilization. Turbulent boundary layers can also be relaminarized by extremely small amounts of distributed wall suction (W. Pfenninger, private communication). If one argues that turbulent fluctuations act on passive inner layers, suction should in fact increase the turbulence by bringing more fluctuations closer to the wall. If, on the other hand, the turbulence is fed primarily as a result of local intermittent instabilities in the innermost region, then removal of this region by slight suction should reduce the turbulence throughout the layer. Such is indeed the case. An explanation for the suppression of turbulent flow by long-chain molecules (polymer additives) has even been offered in terms of the streaks; Gadd (1965) suggested that the long-chain molecules act to inhibit the bursting of the low-speed streaks away from the wall. Other evidence supporting the importance of the streak breakup processes is cited in (I).

If the wall-layer streaks are important to turbulence production, they should not appear in a wall-bound turbulent flow in which there is no production of new turbulence. Such a flow was recently studied by Uzkan & Reynolds (1967). They passed a uniform stream through a grid, and then passed the resulting uniform turbulent flow over a wall moving at the flow speed. This allowed turbulence to be impressed upon a solid wall in the absence of a mean velocity gradient. Hot-

† Note added in proof. Our recent measurements of the instantaneous values of $-u'v'$ confirm that the bursting process indeed contributes the large values; details to be reported separately.

‡ Halleen & Johnston, (1967).

wire studies showed a simple attenuation of the turbulence by the viscous action near the wall, and visual studies showed no evidence of wall-layer streaks. Then, the wall speed and mean speed were mismatched slightly; wall-layer streaks appeared, and the turbulence intensity near the wall actually became greater than that of the impressed turbulence; these observations provide further evidence for the association between streak behaviour and turbulence production.

Some remarks on the relationship of the observed streak phenomena with quantitative studies by other investigators is in order. Previous experimental studies of the energy balance in turbulent boundary layers (see Townsend 1956) have indicated that dissipation of turbulence energy exceeds production in the wake region, and that the necessary supply of turbulent energy is supplied by export from the inner region. It is this supply which keeps the boundary layer in a turbulent state; it is less than either the production or dissipation in the wake region, but is clearly crucial to the maintenance of the turbulent layer. We believe that the streak-ejection process is a dominant contributor to this energy export process. Measurements (though perhaps less accurate) also indicate that there is very little energy transfer from the region $y^+ < 20$ to the region beyond. Hence the source of turbulent energy lies outside of this region. This is consistent with our observation that the streak breakup begins around $y^+ = 30$, and extends outwards along the ejection trajectory. The general nature of these trajectories seems consistent with the space–time correlation measurements of Favre and his co-workers (Favre, Gaviglio & Dumas 1957, 1958). The general structure observed in the viscous sublayer is also consistent with the recent hot-wire explorations of Bakewell & Lumley (1967); they suggest that the motions yielding strong longitudinal vorticity (i.e. the wall-layer streaks) are the dominant ('big') eddies in the wall-layer region. In summary, we know of no reliable experimental data which are inconsistent with our stated conjecture on the importance of the wall-layer streaks.

In summary, we view the formation of wall-layer streaks as the result of vortex stretching due to large fluctuations acting on the flow near a smooth wall† in the presence of strong mean strain. We believe that the production of turbulence near the wall in such a flow arises primarily from a local, short-duration, intermittent dynamic instability of the instantaneous‡ velocity profile near the wall. This instability acts not to alter the mean field flow but rather to maintain it. The ejection of fluid away from the wall in the subsequent process is felt to be the central mechanism for energy, momentum, and vorticity transfer between the inner and outer layers.

This study was financed jointly by the National Science Foundation and the Mechanics Division of the Air Force Office of Scientific Research; their support is gratefully acknowledged. Professor J. P. Johnston provided many helpful suggestions and criticisms throughout the work.

† Observations on rough walls and in free shear flows show different structures and should be considered distinct from the remarks here on smooth walls.

‡ The *mean* velocity profile is believed to be stable to small disturbances (Reynolds & Tiederman 1967).

## REFERENCES


BAKEWELL, H. & LUMLEY, J. 1967 To appear in *Phys. Fluids.*

BETCHOV, R. & CRIMINALE, W. 1964 *Phys. Fluids* **7**, 1960.

BLACK, T. J. 1966 *Proc. Heat Transfer and Fluid Mech. Institute*, p. 336. Stanford University Press.

BLACKMAN, R. B. & TUKEY, J. W. 1959 *The Measurement of Power Spectra.* New York: Dover.

CANNON, J. 1965 Ph.D. Dissertation, Mech. Engrg Dept., Stanford University.

CLAUSER, F. H. 1956 *Advances in Applied Mechanics*, vol. IV, p. 2. New York: Academic Press.

COMTE-BELLOT, G. 1963 *J. Mécanique*, vol. II, no. 2.

ELDER, J. W. 1960 *J. Fluid Mech.* **9**, 235.

FAVRE, A., GAVIGLIO, J. & DUMAS, R. 1957 *J. Fluid Mech.* **2**, 313.

FAVRE, A., GAVIGLIO, J. & DUMAS, R. 1958 *J. Fluid Mech.* **3**, 344.

GADD, G. 1965 *Nature, Lond.* **206**, 463.

HALLEEN, R. M. & JOHNSTON, J. P. 1967 *Rept. M. D.* 18, *M. E. Dept., Stanford University.*

KAYS, W. M. & MORETTI, P. M. 1965 *Int. J. Heat and Mass Trans.* **8**, 1187.

KLEBANOFF, P. S. 1954 *NACA TN* 3178.

KLEBANOFF, P. S., TIDSTROM, K. D. & SARGENT, L. M. 1962 *J. Fluid Mech.* **12**, 1.

KLINE, S. J. 1964 *Flow Visualization* (16 mm motion picture), Educational Services, Inc., Newton, Mass.

KLINE, S. J. 1965*a* *Proc. Inst. Mech. Engrs.* **180**, part 3J.

KLINE, S. J. 1965*b* *Gen. Motors Symp. on Internal Flow.* Amsterdam: Elsevier.

KLINE, S. J. & RUNSTADLER, P. W. 1959 *Trans. ASME* (Ser. E), no. 2, 166.

KOVASNAY, L. S., KOMODA, H. & VASUEDVA, B. R. 1962 *Proc. Heat Transfer and Fluid Mech. Institute*, p. 1. Stanford University Press.

LAUFER, J. 1951 *NACA Rept.* 1053.

LAUFER, J. 1954 *NACA Rept.* 1174.

LAUNDER, B. E. 1964 *M.I.T. Gas Turbine Lab. Rept.* 77.

LIGHTHILL, M. J. 1963 *Laminar Boundary Layers*, p. 99 (ed. L. Rosenhead). Oxford: Clarendon Press.

LIU, C. K. 1966 *Mech. Engrg Dept. Rept.* MD-15, Stanford University.

MEYER, K. A. & KLINE, S. J. 1961 *Mech. Engrg Dept. Rept.* MD-7.

MEYER, K. A. & KLINE, S. J. 1962 *A Visual Study of the Flow Model in the Later Stages of Laminar–Turbulent Transition on a Flat Plate* (16 mm motion picture), Cat. no. M-3, ASME Film Library.

MOORE, C. & KLINE, S. J. 1958 *NACA TN* 4080.

REYNOLDS, W. C. & TIEDERMAN, W. G. 1967 *J. Fluid Mech.* **27**, 253.

RUNSTADLER, P. W., KLINE, S. J. & REYNOLDS, W. C. 1963 *Mech. Engrg Dept. Rept.* MD-8, Stanford University.

SABIN, C. M. 1965 *Trans. ASME* (Ser. D), no. 2, p. 421.

SANDBORN, V. 1953 *NACA TN* 3013.

SCHRAUB, F. A. & KLINE, S. J. 1965*a* *Mech. Engrg Dept. Rept.* MD-12, Stanford University.

SCHRAUB, F. A., KLINE, S. J., HENRY, J., RUNSTADLER, P. W. & LITTELL, A. 1965*b* *Trans. ASME* (Ser. D), **87**, 429.

STUART, J. T. 1965 *NPL Aero. Rept.* 1147.

TOWNSEND, A. A. 1956 *The Structure of Turbulent Shear Flow.* Cambridge University Press.

UZKAN, T. & REYNOLDS, W. C. 1967 *J. Fluid Mech.* **28**, 803.